Review of Literatures

Chapter 2 Review of Literatures

Ionizing radiations due to their application in various domains have good impact on everyday human life. At the same time, ionizing radiation, also due to ionizing properties, affects human life negatively by posing a risk for the deterministic and stochastic biological effects. Radiation detectors are required to (i) measure the radiation dose for particular application and (ii) ascertain that the dose of the radiation worker is limited below the permissible limits. This chapter discusses the ionizing radiation sources and their application, the interaction of ionizing radiation with matter and radiation detection and measurement mechanism. An extensive review of different structures of ZnO and TiO_2 along with synthesis method and device for radiation detection and measurement are discussed.

2.1 Ionizing Radiation: Sources and Application

Radiation is the energy traveling in space and is broadly classified into two types. The radiation which is not capable of ejecting electrons from atoms and molecules and the energy transfer only results in vibration, rotation of molecules (radio, microwaves & IR) or electronic excitation (Visible & UV) and is known as "Non-ionizing Radiation" (figure 2.1a). The other category consists of radiation with sufficiently high energy that can eject electrons from atoms of the medium, i.e., it can ionize the medium and is referred as "Ionizing Radiation" (figure 2.1b). Theoretically, radiation with energy >10 eV is known as Ionizing radiation. Ionizing Radiation can be high-energy electromagnetic radiation (X-rays & Gamma Rays) or Particles (Alpha, Beta, Neutrons, Protons and other heavy charged particles).

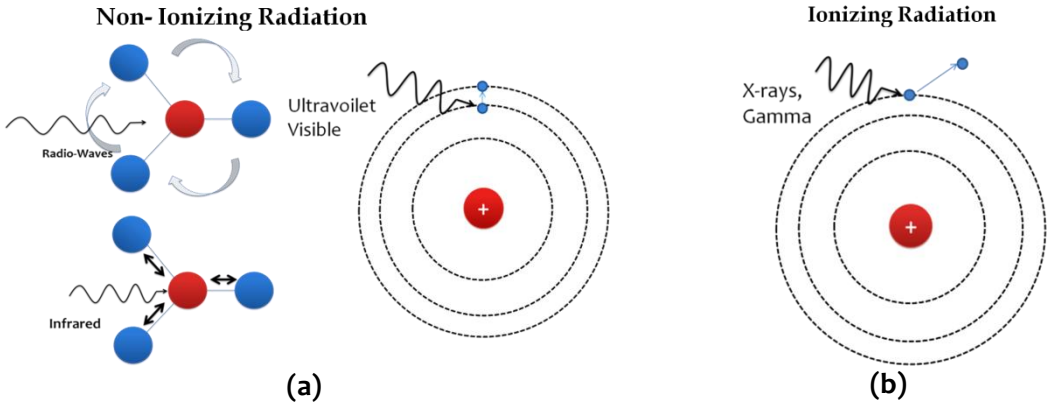

Figure 2.1: Non-Ionizing Radiation (Radio waves-UV) results in molecular rotation, vibration and electronic excitation and Ionizing Radiation (X rays, Gamma rays) can eject electrons from atoms

These radiations are produced spontaneously from unstable nuclei called radioactive decay. These radioactive materials are either naturally present on the earth or can also be produced artificially. Theses radiation from space also reaches the earth from cosmic nuclear reactors such as stars employing nuclear fusion reaction liberating different kinds of radiation. Space radiation, when interacting with the earth environment, generates numerous particles. Man-made sources, i.e., X-ray generating machine, accelerators also produce such radiations

2.1.1 Sources of Ionizing Radiation:

2.1.1.1 *X-rays*

X-rays are the first Ionizing Radiation detected in 1895 by W. Roentgen when studying the cathode rays (electrons) generated in the cathode ray tube. This tube consisted of two electrodes in low-pressure atmospheric gas; electrons are emitted due to the high voltage applied across the tube. Roentgen noticed 'unknown rays' emitted from the anode due to the strike of high-energy electrons on the anode and named X-rays. Roentgen tube was the first ionizing radiation generating equipment. Later modern Coolidge tube was designed for generation of X–rays for a practical purpose (figure 2.2 a). X-rays are basically generated in two ways; stopping an electron in matter causes resulting in emission of breaking radiation or Bremsstrahlung. These radiations have broad spectrum of energy and referred as 'continuous x rays. the other way generating x rays is ejection of core electron and subsequent transition of outer orbit electron to core level releasing X-rays with a fixed wavelength called 'characteristic X-rays. Both types of X-rays depend on the material used as a target to generate it (figure 2.2b).

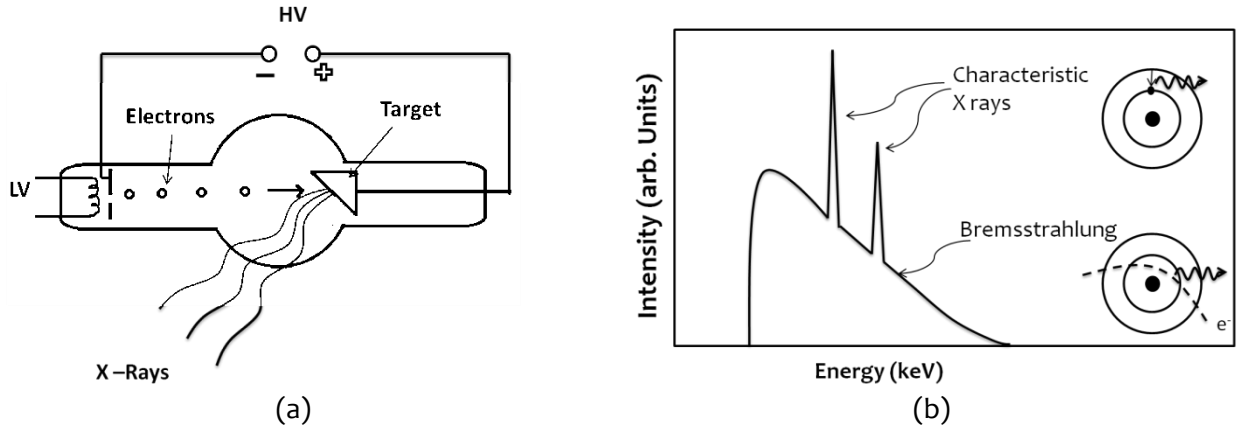

Figure 2.2: (a) Schematic diagram Coolidge tube (b) The generated X-ray has characteristics and Bremsstrahlung

X-rays are the highest energy radiation involves atomic interaction with electron. Another radiation called Gamma radiation which has higher energy than X-rays are generated from nuclear transitions.

2.1.1.2 *Gamma Rays*

An excited nucleus releases a high-energy electromagnetic wave called 'Gamma rays'. This excited nucleus is found in radioactive materials occurring naturally or can be prepared in a nuclear reactor. Naturally occurring radioactive materials (NORM) consists of radioisotopes of the element present in earth crust such as ^{238}U, ^{232}Th, ^{226}Ra, ^{222}Rn, ^{40}K, etc. and continuously emit heavy/light charged particle and high energy gamma rays from unstable nuclei. These radiations also come on earth from the solar system and distant galaxies called 'cosmic radiation'. Terrestrial and cosmic radiation constitutes weak intensity radiation on earth called 'Background radiation'. Gamma radiation ranges from 50 keV-10 MeV. Apart from these naturally occurring materials, radioactive materials can also be prepared in a nuclear reactor such as ^{137}Cs, ^{60}Co, etc., which generate high energy gamma rays 662 keV and 1.17 and 1.33 MeV gamma radiation. Figure 2.3 shows the decay scheme of ^{137}Cs and ^{60}Co. Beta-decay of ^{137}Cs results in Ba, which is often in excited state and on relaxation, it emits 662 keV gamma radiation. Similarly, beta decay of ^{60}Co leads to the production of excited ^{63}Ni, which emit 1.33 and 1.17 MeV of gamma radiation.

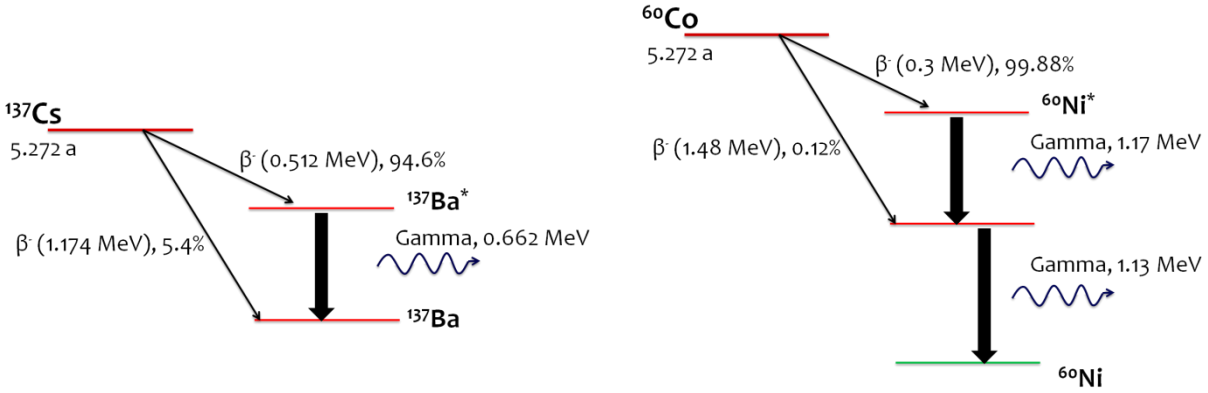

Figure 2.3: Decay Scheme of ^{137}Cs and ^{60}Co Gamma radiation source

2.1.1.3 *Alpha Radiation*

Alpha particles are emitted from the heavy nucleus of transuranic elements because of a high atomic mass nucleus; Columbic repulsion dominates the nuclear binding forces. Alpha particle emitted in this process leaves the parent nuclei with a deficiency of 2 protons and 2 neutrons. After emission, if N/Z ratio matches with the stable value, it will not radiate but if there is a slight deviation, it will lead to the conversion of neutron into proton or vice versa with emission of beta particle (e^- or e^+) as this may stabilize their N/Z ratio. Figure 2.4a shows the decay scheme of ^{241}Am alpha source, showing the emission of alpha particle with different energies and consequent gamma emission due to relaxation of excited daughter product. Alpha particle is also produced in various nuclear reactions such as D-T reaction, Neutron capture reaction with ^{6}Li and ^{10}B isotopes. D-T reaction is used for neutron generation and alpha particle comes as a byproduct (figure 2.4 b). This alpha particle emits exactly opposite to the neutron and thus alpha detection is used in imaging applications. D-T reaction is also used for power generation in Fusion reactor and alpha particle measurement to ascertain the plasma confinement.

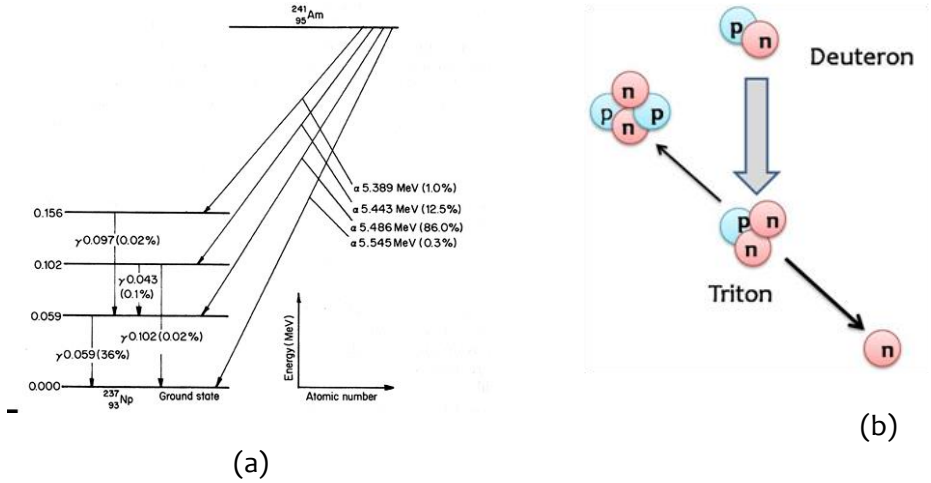

Figure 2.4 (a) Alpha and Neutron Emission in D-T reaction (b) Spontaneous Alpha particle emission from radioactive ^{241}Am nucleus

2.1.1.4 *Beta Radiation*

Beta particles are high-energy electrons/positron with energy ~ keV-MeV emitted from the radioactive nucleus to stabilize the N/Z ratio. A nucleus containing large no. neutron then it goes for beta minus (β-) decay $\rightarrow p + e^- + \bar{\nu}$. Similarly, if number of protons is higher beta plus

(β^+) decay occurs $p \rightarrow n + e^+ + \nu$. Most beta emitters emit gamma radiation as a result of relaxation of daughter product (See section 2.1.1.2), but few are called "pure beta emitters", which do not emit gamma radiation. Because of neutrino/antineutrino emission and beta particles, the decay energy is shared between two particles that may not be the same for any given decay; hence, emitted beta particles are not monoenergetic but have a range of energies (figure 2.5a). Another process of emission of the beta particle is "Internal conversion", in which nuclear excitation energy is directly transferred to K shell or M shell electron, leading to the emission of nearly monoenergetic electrons (figure 2.5b)

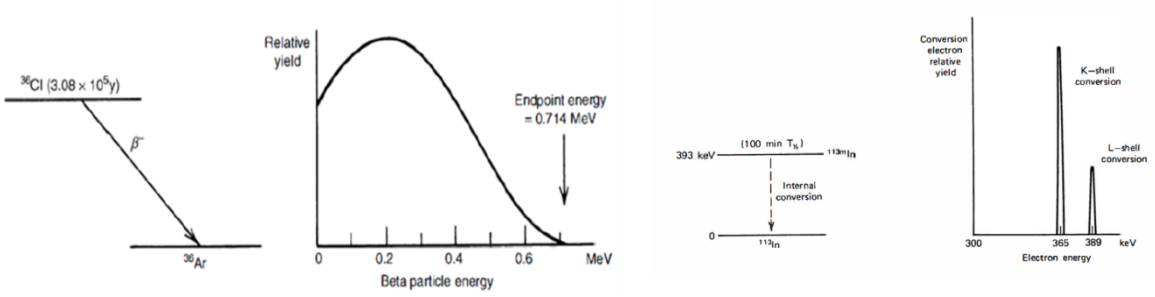

(a) (b)

Figure 2.5: (a) Decay scheme and energy spectrum of ^{36}Cl beta decay (b) Decay scheme of ^{113}In and energy spectrum of Beta particle from internal conversion (Knoll, 2010)

2.1.1.5 *Neutron Radiation*

Neutrons are uncharged particles emitted in spontaneous fission from a radioactive nucleus (^{252}Cf) in which a very high Z and A nucleus fragments itself to create two smaller nuclei. In this process, few neutrons are also emitted along with fission fragments (figure 2.6 a). Neutrons can also be generated from a nuclear reaction such as D-T or D-D reaction. In these reactions, monoenergetic neutrons are generated. Another source of the neutron is (Alpha, n) reaction in which alpha particles are allowed to incident on target such as beryllium (^{9}Be) results in the emission of neutrons ranging from 100keV-10 MeV using reaction ${}^4_2\text{He} + {}^9_4\text{Be} \rightarrow {}^{12}_6\text{C} + {}^1_0\text{n} + \gamma$. The daughter product Carbon often is in excited states which relaxes by emitting gamma radiation 4.5 MeV (figure 2.6 b)

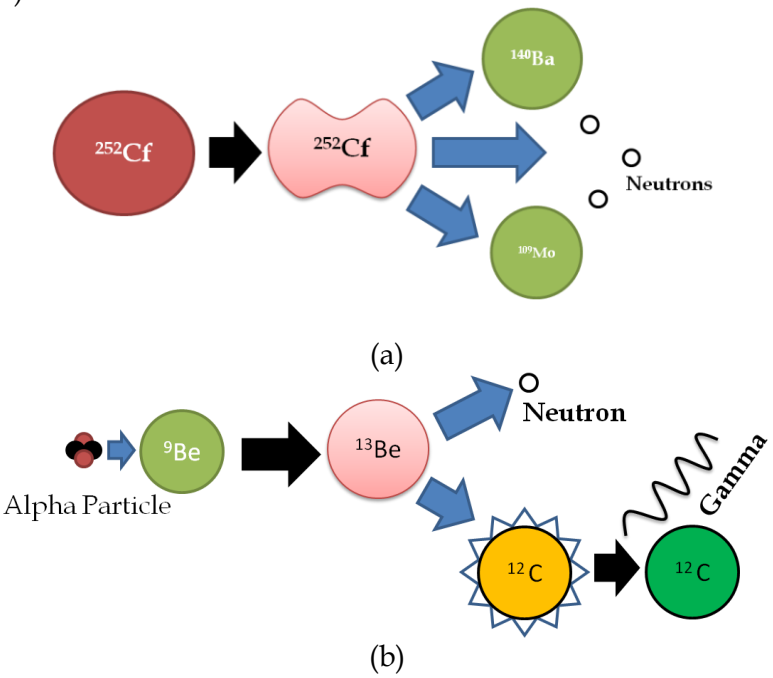

Figure 2.6: Neutron emission using (a) Spontaneous Fission (b) (Alpha, n) reaction

2.1.1.6 *Proton and Heavy Charged Particles*

High energy protons and other heavy charged particles are generated using linear accelerators, which consist of cylindrical hollow electrodes kept at alternatively variable potential and synchronized with the motion of proton through it such that it will experience a force leading to its acceleration. Accelerators produce energy of the order of several MeV (Figure 2.7).

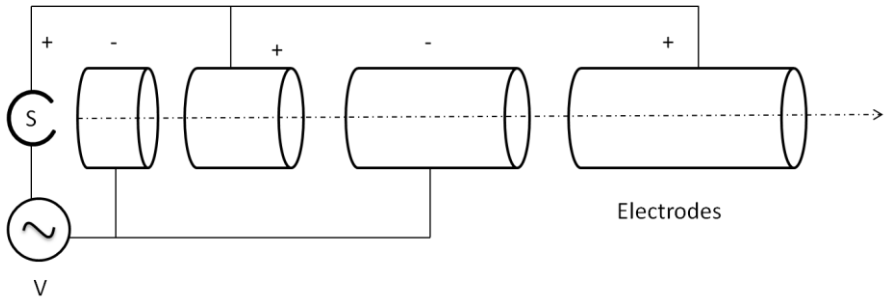

Figure 2.7: Schematic diagram of Linear accelerators

Table 2.1 summarizes the different types of ionizing radiation, sources and respective energies.

Table 2.1: Sources and Types of Ionizing Radiation

Radiation	Sources	Process	Energy
X rays	Coolidge tube	Electron Stoppage in Target	1keV-50 keV
Gamma Rays	Radioactive Material	Nuclear Energy Transition	50 keV-10 MeV
Alpha Radiation	Radioactive Material	Alpha Decay of high Z material, D-T Rection, (n, α) rection	4-8 MeV
Beta Radiation	Radioactive Material	Beta Minus decay, Beta plus decay and electron capture	10 keV-2 MeV
Neutron	Radioactive Material Nuclear Reaction	Spontaneous Fission D-T, D-D, (α, n) reaction	0.025-20 MeV
Proton	Linear Accelerator	Proton acceleration	~MeV

2.1.2 Applications of Ionizing Radiation

Ionizing radiation due to its ionizing characteristics is used in many domains such as Industry, Medicine, Agriculture and research application. In medicine, these radiations are used for radio therapy applications as radiation can kill the cells. Charged particles (alpha, proton) have an advantage over the x ray and gamma rays as charge particles lose the energy precisely with minimum damage of other living cells surrounding the tumor. X-rays are used for the diagnosis of bones and brain tumors using computed tomography. Also, it is used for determining crystal structures and elemental composition using XRF and internal structures of components using radiography. Gamma radiation is used in sterilization of medical products. It inhibits the sprouting in agricultural products, also used in polymerization using radiation-

induced cross-linking due to radical produced by the radiation exposure. Waste water or sludge dis-infection is another area of application of gamma radiation. Alpha sources are used to ionize the air, various gauges for pressure, density, thickness and humidity. Alpha bombardment on Be target results in the production of neutrons using (alpha, n) reaction and widely used as a large half-life neutron source, which is used for alpha radiation produced in D-T reaction in a fusion reactor and neutron generator. Measurement of these alpha particles ensures the plasma confinement in the reactor. Alpha emitted in opposite to neutrons in a neutron generator is used to map the position of neutrons and turn the material under interrogation. Thermo-electric generator is another application of alpha source. Heat dissipated by alpha particles converted into electricity works as a long-lasting power supply in long space missions. Beta sources are used in Brachytherapy, another type of radiotherapy in which a source is placed near the tumor inside the body, leading to fast treatment compared with external beam radio therapy (EBRT). Beta sources are also used in the thickness control of papers and radioactive tracers. Neutron exposure is used to create artificial radioactive sources, explore oil and minerals, gauges and control nuclear materials and Radiography. Figure 2.8 summarizes the applications of various ionizing radiations.

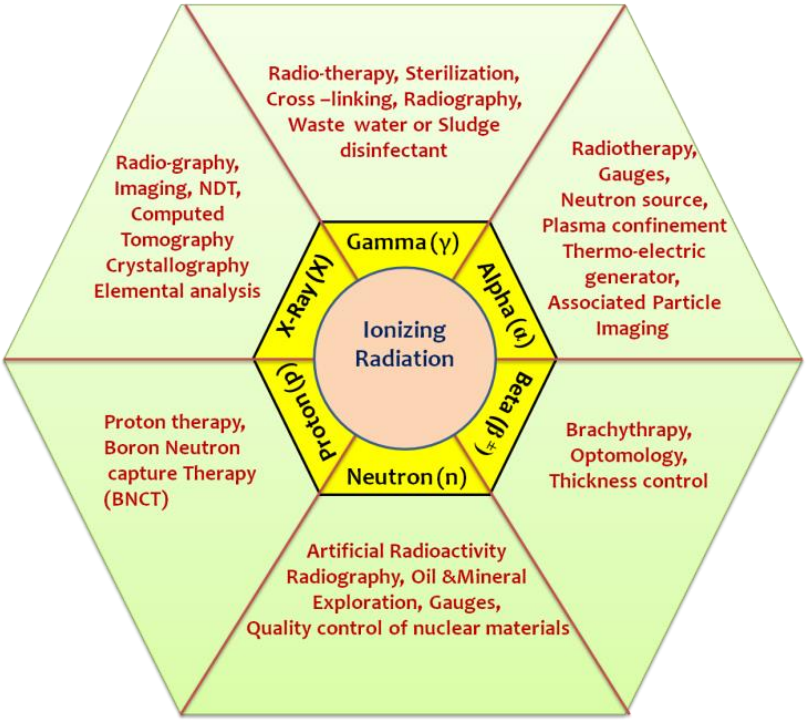

Figure 2.8: Application of Ionizing Radiation

2.2 Mechanism of Ionizing Radiation Energy Absorption

2.2.1 Alpha Particles and Heavy Charged Particles

Charged particle when enters in any medium, primarily interact via Columbic force with the electron or nucleus of atoms of the materials. When the energy of the particles is sufficiently high and the interaction medium is composed of high Z atoms, then another mechanism comes into the picture called radiative loss, in which particle retarded by the nucleus leading to the emission of electromagnetic radiation called Bremsstrahlung (breaking radiation). Alpha particles are charged massive particles (m=4.0 amu and Z=+2e). Due to its electrical charge, it strongly interacts with atomic electrons. While passing in medium, it exerts Columbic force on the electrons present in the medium, resulting in elevation of electron energy within the atom,

i.e., excitations of the atoms or liberation of electrons from atomic orbital, i.e., ionization of the medium. The maximum energy transferred to an electron of mass m_e in a single collision with a charged particle of mass M and kinetic energy E is given by 4 Em_e/M (Knoll, 2010). Charged particle with energy E loose its energy continuously while passing in a medium, referred to as stopping power of the medium. Stopping power of material of atomic number Z for charge particle of charge +ze is;

$$-\left(\frac{dE}{dx}\right)_{Coll.(electronic)} = \frac{4\pi z^2 e^4}{mc^2\beta^2} NZ\left[ln\frac{2mc^2\beta^2}{I(1-\beta^2)} - \beta^2\right]$$

$$-\left(\frac{dE}{dx}\right)_{Coll.(nuclear)} = \frac{N\pi Z\ ze^4}{E}\left(\frac{m}{M}\right) ln\left(\frac{\gamma E}{E_d}\right)$$

Where N is atomic number density, $\beta = v/c$ velocity of the particle relative of light c, m is the particle's mass. γ is a constant, M is the mass of the nucleus of the target atom. Stopping power of air for the alpha particle of different energies calculated by SRIM software is shown in figure 2.9 a. It is evident that large stopping power is due to the electronic integration (black curve) and a small contribution of nuclear stopping power (red curve) because alpha particles mostly interact with atomic electrons. The range of 5.5 MeV Alpha particle in the air is ~41 mm. (Ziegler et al., 2010)

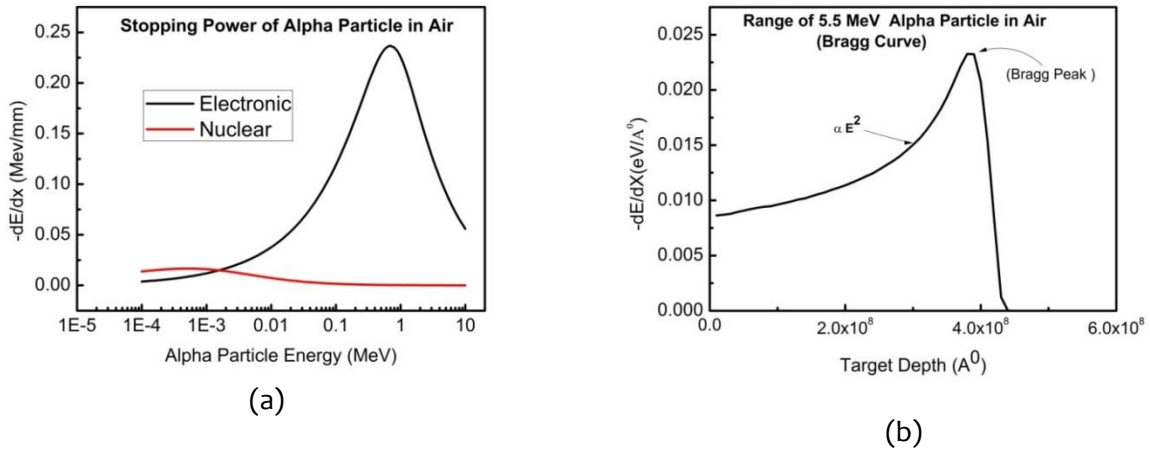

Figure 2.9 : (a) Stopping power of alpha particle of different energies in air (b) Range of 5.5 MeV alpha particle in the air (Calculated from SRIM Software, 2010(Ziegler et al., 2010))

2.2.2 Beta Particles

Beta particles have mass ~1800 times lower than alpha particles, thus greatly deflected during the collisional interactions with electrons. Other than the collisional loss of energy, beta particles tend to lose via radiative process due to their de-acceleration by the nucleus called 'bremsstrahlung'. Thus, stopping powder consists of two parts;

$$\frac{dE}{dx} = \left(\frac{dE}{dx}\right)_{coll\ (electronic)} + \left(\frac{dE}{dx}\right)_{rad}$$

$$\left(\frac{dE}{dx}\right)_{raditive} = NE\sigma_{rad} = \frac{NEZ(Z+1)e^4}{137m_0^2c^4}\left(4ln\frac{2E}{m_0c^2} - \frac{4}{3}\right)$$

The stopping power of beta particles of different energies in the lead (Pb) is calculated from ESTAR Program (NIST, n.d.) is shown in figure 2.10. For smaller energies, energy loss is due to collisional interactions. As the energy increases by 500 keV, radiative interactions become significant, rising with an increase in energy.

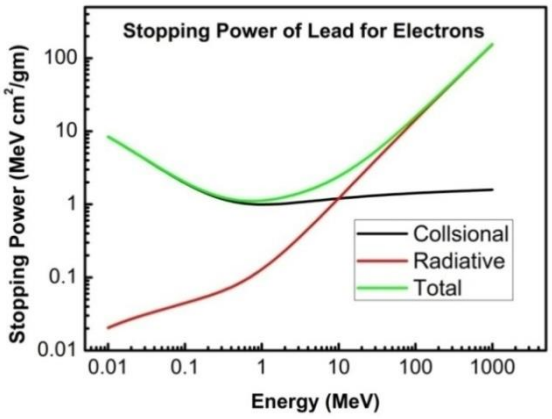

Figure 2.10: stopping power of electrons of various energies in Lead (Pb) target(NIST, n.d.)

2.2.3 Neutrons

Neutrons are uncharged particles having range of energy ~0.025 -20 MeV. Due to uncharged nature, it does not interact with the orbital electrons of the target atoms like a charged particle. It only interacts with nuclei of target atoms in three ways which depend upon energy, Absorption or capture, Elastic scattering and Inelastic Scattering. These are described in the following subsections.

2.2.3.1 Neutron Capture

Low energy neutron when incident on target material, absorbed by the nuclei of target material making compound nucleus which lasts in time ~10^{-14}s and decays into two smaller nuclei. The energy released during this process is a result of the mass difference of parent and daughter nuclei. The released energy is distributed among the nuclei created after the reaction (figure 2.11a). The probability of capture of the neutron, i.e., capture cross-section, depends upon the neutron energy and mass number of isotopes. Certain isotopes have high capture cross-sections such as ^{3}He, ^{6}Li, ^{10}B and ^{235}U and used converter materials to detect and measure neutrons. Figure 2.11 b shows the cross-section for these isotopes at different energies. As the energy of the neutron increases, the capture cross-section drastically decreases.

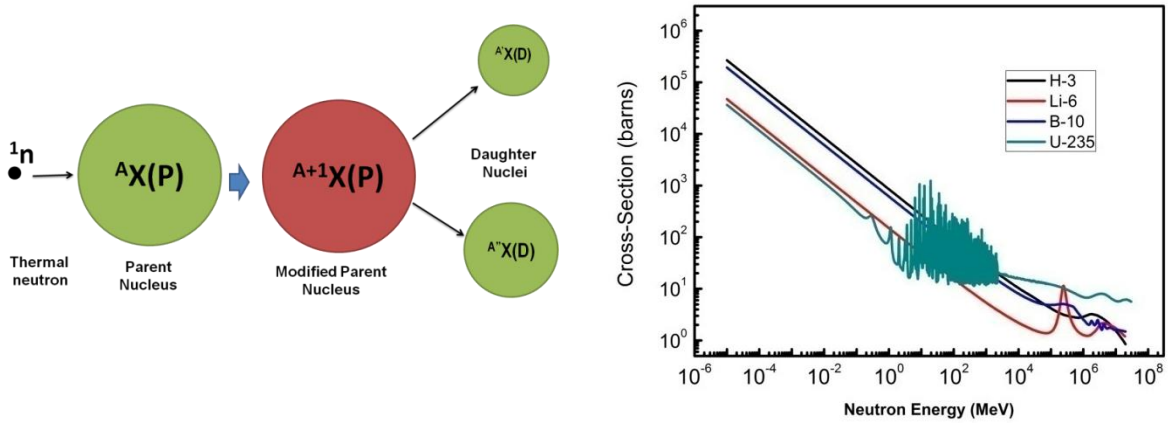

Figure 2.11: (a) Neutron Capture in ^{6}Li results in formation of ^{3}H and ^{4}He (b) Scattering cross-section of few isotopes (JANIS Data)

2.2.3.2 *Neutron Elastic Scattering*

Fast Neutrons will have less probability of capture, so they scatter from the nuclei. Neutron with energy E_n incident on the nucleus is elastically scattered with energy E'_n and energy difference $E_x = (E_n - E'_n)$ is transferred to the nucleus as kinetic energy (figure 2.12). The recoiled nucleus further travels in the material, depositing all its kinetic energy from scattered neutrons into the medium. The energy transferred by neutron scatted at angle θ is

$$E_X = \frac{4A}{(A+1)^2}\cos\theta\, E_n$$

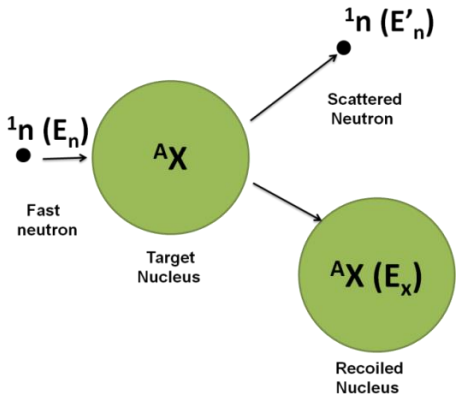

Figure 2.12: Elastic Scattering of Neutron

The recoiled energy is highly dependent on the scattering angle for given neutron energy and is maximum at $\theta=180^0$. It also depends on the atomic mass of the target nuclei A. The recoiled energy is maximum for hydrogen; that is why hydrogenous material such as wax is used to shield the material.

2.2.3.3 *Inelastic Scattering*

When the energy of a neutron is very high, it scatters from the nuclei in-elastically transferring some energy to nucleus by which it gets excited. The excited nuclei may release extra energy by releasing gamma radiation (figure 2.13).

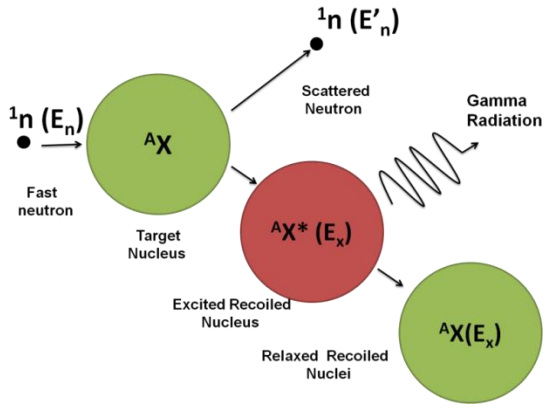

Figure 2.13: Inelastic Scattering of neutron

2.2.4 X rays and Gamma Radiation

When ionizing radiation passes through any material, it deposits its energy by scattering and absorption in the materials. The deposition of energy in the matter depends upon the effective

Z, energy and type of radiation. Electromagnetic radiation, such as gamma, X-rays, interacts through (i) **Photoelectric absorption**, i.e., the X- or gamma-ray photon vanishes during its interaction with atomic electron and transfers all the energy to the electron, (ii) **Compton scattering** where the partial energy transfer takes place (iii) and **Pair production** when the energy of the photon is very high (>1.02 MeV), This absorption of high-energy photons results in the production of one pair of electron and positron. The positron, being an antiparticle, annihilates itself when it finds an electron in the material (figure 2.14). The cross-section for different interaction mechanisms depends upon the Z of the target and the energy of the photon.

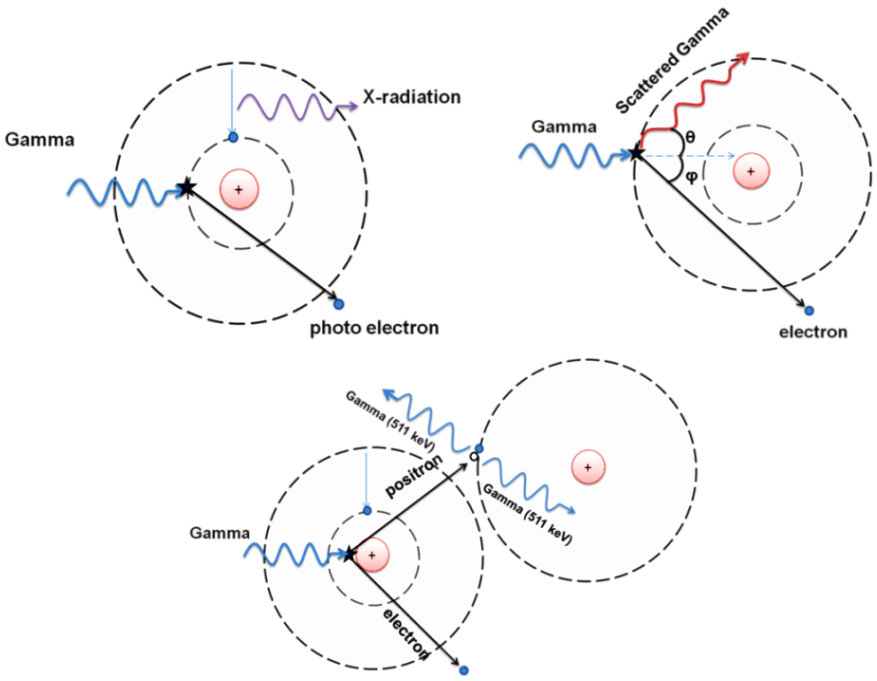

Figure 2.14: Interaction of Gamma Radiation in three different ways depending upon the energy of radiation and Z of material.

The cross-section for the photoelectric absorption process is $\sigma_{PE} \alpha \frac{Z^5}{E^{3.5}}$; which dominates for low energy photons and high Z target material. Compton scattering cross-section $\sigma_{CS} \propto \frac{Z}{E}$, less dependence on Z and E effective for intermediate energies 500 keV-1 MeV and low Z material such as water, human tissue. Pair production cross-section $\sigma_{PP} \propto Z^2 \ln E$; requires threshold energy of 1.02 MeV and dominates on very high energy and high Z material.

2.3 Radiation Quantities

Radiation can be measured in two ways; (i) Activity of radioactive material. (ii) Radiation energy absorbed per unit mass, i.e., radiation dose. Activity is measured in case of radioactive contamination in air, liquid, surface, etc. Radiation dosimetry is carried out for environmental, radiation protection, medical, industrial and other applications. When ionizing radiation is incident on a medium, either it directly ionizes the medium or transfers the energy to create secondary particles that further travel in the medium and deposit their energy to the medium. The medium may be air, tissue, or any solid material of interest and depending upon the type of radiation and its interaction, various radiation quantities are defined accordingly.

2.3.1 Activity (A):

The number of decays per second of a radioactive source is termed its Activity. Mathematically it is defined as $A = -\frac{dN}{dt}$, where dN is the change rate of existing nuclei in dt time. N is the total number, decays exponentially with time as $N = N_0 e^{-\lambda t}$. The activity A can be expressed as $A = -\lambda N$. The unit of activity is 'Bq' defined as 1 Becquerel (Bq) = one disintegration or decay per second. The old unit of activity is Curie and is defined as 1Ci = 3.7×10^{10} Bq, which is equivalent to the activity of 1g of Ra-226.

2.3.2 Kinetic Energy Released Per Unit Mass (KERMA)

Indirect ionizing radiation such as X rays, Gamma and Neutrons produces secondary particles such as electron, proton and recoiled nucleus on interaction with a medium that further interacts with medium atoms. The initial kinetic energy transferred per unit mass to these secondary particles is defined as "KERMA". Mathematically,

$$K = \Delta E / \Delta m$$

Where ΔE is kinetic energy transferred in Δm mass exposed to radiation. Medium of area ΔA with mass Δm exposed to radiation with Energy fluence Ψ_E. If the density of the medium is ρ and mass–energy transfer coefficient is μ_{tr}, then energy transfer can be written as

$$\Delta E = (\Psi_E \Delta A) * \left(\frac{\mu_{tr}}{\rho}\right) * \left(\frac{\Delta m}{\Delta A}\right) = \Psi_E \frac{\mu_{tr}}{\rho} \Delta m$$

$$\boldsymbol{K = \Psi_E \frac{\mu_{tr}}{\rho}}$$

Unit of KERMA is J/kg or Gy (Gray)

2.3.3 Absorbed Dose (D)

The radiation dose to a medium is defined as the energy absorbed per unit mass of the medium. If the energy absorbed within the mass Δm is ΔE, the absorbed dose D defined as:

$$D = (\Delta E / \Delta m)$$

Unit: J Kg^{-1} or Gray (Gy)

Although dose and KERMA have the same physical dimension, qualitatively, both are not the same. For absorbed dose ΔE, account for the energy dissipated within Δm, not only by the charged particles produced by photon interactions within Δm, but also by those originating outside Δm and passing through Δm.

2.3.4 Equivalent Dose ($D_{Eq.}$)

Radiation energy absorbed in the biological medium like the human body results in deterministic/stochastic effects, which are not same for all types of radiation because of differences in the interaction. Therefore, a radiation weighting factor (W_R) multiplied to absorbed dose in Gy to make the dose equivalent. Equivalent dose is measured in Sievert (Sv)

$$D_{Eq.}\,(Sv) = D(Gy) * W_R$$

Radiation weighting factor varies from 1-20 depending on the type of radiation as below;

Radiation	**Weighting factor (W_R)**
Beta, Gamma, X rays	1
Proton	2
Neutron	2-20 (depending on energy)
Alpha particle and Heavy charged particle	20

2.3.5 Effective Dose

In the case of radiation exposure to a human body, the biological effects also depend upon the radiosensitivity of the individual organ. The effective dose of particular organ can be obtained by multiplying the tissue weighting factor to the equivalent dose received by the organ;

$$\text{Effective dose } D_{Eff}\,(Sv) = \Sigma\, D_{eq.}(Sv) * W_T$$

Where W_T is the tissue weighting factor of different tissues tabulated in table 2.2

Table 2.2: Tissue Weighting Factors of Human Tissues

Tissue	*Weighting factor* W_T	$\sum W_T$
Bone-marrow (red), Colon, Lung, Stomach, Breast, Remainder Tissues**(nominal weighting factor applied to the average dose to 14 tissues)	0.12	0.72
Gonads	0.08	0.08
Bladder, Esophagus, Liver, Thyroid	0.04	0.16
Bone surface, Brain, Salivary glands, Skin	0.01	0.04

Those organs, which multiply at a very fast rate, are relatively more sensitive to ionizing radiation.

2.3.6 Biological Effects of Ionizing Radiation Exposure

Radiation exposure to human can take place due to (1) Cosmic and terrestrial background radiation, (2) Medical diagnosis involving ionizing radiation, (3) routine radiation work in the laboratory, (4) External exposure due to accidental release of radioactivity in the environment, (5) Internal contamination due to airborne radioactivity due to accident and (6) direct and indirect contamination due to ingestion of contaminated food. Cell is the basic building block of a biological organism. The human cell is of the size ~10 μm consisting of a nucleus, consisting of chromosomes made of DNA. Ionizing radiation such as Alpha, Beta, Gamma and Neutron when interacting with a cell nucleus, can damage DNA in two ways: (1) either direct damage or (2) it may interact with water molecules producing free radicals of H^+, OH^-, H_3O, etc. which interact with DNA. In each case, the damaged DNA of the cell may repair itself correctly, leading to no effect on the cell or could not repair correctly, leading to cell death. Death of cell leads to deterministic impacts, which are certain after a threshold dose and mis repair of the cell

leads to alteration in the normal functioning of a cell resulting in stochastic effects such as carcinogenesis or genetic effects or mutation. These effects do not require any threshold dose and may happen at any dose.

2.3.6.1 *Deterministic Effects*

NVD (Nausea, Vomiting and Diarrhea) syndrome, death, epilation, skin erythema and sterility and cataract are examples of deterministic effects. All the above effects are immediate, excluding cataract, which is a delayed effect. Table 2.3 and 2.4 summarize the dose range and their impact on whole body exposure and local exposures.

Table 2.3: Deterministic Effects due to whole-body irradiation at different Radiation Doses(Valentin, 2007)

Dose range		Effects
(Sv)	(Rem)	
0.1	<10	Non detectable
0.1 to 1	10 to 100	Chromosomal Aberrations
1 to 3	100 to 300	Nausea, Vomiting, Diarrhea (NVD), Loss of Appetite. (Recovery probable)
3 to 5	300 to 500	More Severe NVD plus fever. Radiation sickness, (recovery probable) LD 50/60* (lethal dose)
>5	>500	Death within a few days to weeks may be due to hematopoietic and gastrointestinal failure.

***** Dose which may result in the death of 50 percent of the irradiated persons within 60 days.

Table 2.4: Deterministic Effects due to Local irradiation at different Radiation Doses

Dose (Sv)	Region	Effects
1.5-2.0	Ovary	Temporary Sterility
2.0-5.0	Ovary	Permanent Sterility
6	Skin	Skin erythema
8	Eye lenses	Cataract (after 5to10 years)
6-10	Tastes	Permanent Sterility
3	Hair Follicles	Epilation
10-20	Skin	Burns, blisters, wounds, death of tissue (necrosis)

2.3.6.2 *Stochastic Effects*

Induction of cancer, leukemia and hereditary effects are examples of stochastic effects. The hereditary effects arise due to gene mutations in the parent, which are transferred to the subsequent generations. Gene mutations have been occurring due to natural causes. Radiation also induces gene mutation. The radiation dose that will induce a mutation rate equal to that due to natural causes alone is called the doubling dose. It is in the range of 0.2-1.0 Sv (20-100 rem). Embryo and fetus are particularly radiosensitive and hence women of reproductive age

are vulnerable to radiation. Most of the delayed effects of radiation, e.g., cancers, hereditary effects are stochastic in nature (radiation-induced cataract is an exception), i. e., they have no threshold dose and the occurrence of the impact has a probability that depends upon the magnitude of the dose received (table 2.5). Based on data obtained on occupational exposure, radiotherapy experience etc., the following probability values (risk factors) are accepted for these stochastic effects.

Table 2.5: Stochastic Effects and the Risk Factor

Effects	Probability (Risk Factor)	
All Cancers (fatal, nonfatal)	5×10^{-2} per Sv	5×10^{-4} per rem
Hereditary effects (first two generations)	1×10^{-2} per Sv	1×10^{-4} per rem

2.4 History of Development of Ionizing Radiation Sensor

The development of ionizing radiation detectors dates back to the discovery of the first ionizing radiation itself, i.e., the discovery of X-rays by W. Roentgen in 1895 while working on cathode rays. Potassium Palatino cyanide, when accidentally struck by X-ray generated by electrons on the anode to crooks tube, made the invisible radiation due to fluorescence thus can be regarded as the first detector of ionizing radiation (Panchbhai, 2015). H. Becquerel one year later, working on the assumption that X-rays can be generated by exposing the sample to the Sun, accidentally discovered other ionizing radiations, i.e., alpha, beta and gamma radiation spontaneously emitted using a photographic plate. The phenomena are known today as "Radioactivity" (Donald Blaufox, 1996). These two discoveries triggered the development of ionizing radiation detectors and since then, numerous efforts are being made continuously to detect ionizing radiation and different types of detectors.

ZnS screen is the earliest detector, introduced by Crookes in 1903 and was used for visual scintillation counting of alpha particles(Kolar and den Hollander, 2004). Gas ionization detector developed in 1930, where ionization produced in gas is converted in the electrical pulse, made visual scintillation counters obsolete. The gas counters are sensitive compared to visual scintillation counting, thus detecting weakly ionizing radiation such as beta and gamma radiations, which could not be detected by visual scintillation counting. Curran and Baker (1944) introduced a device called photomultiplier tube (PMT), in which a photon is converted into an electrical pulse by electron multiplication. It was used by Blau and Dreyfus (1945) to demonstrate that the increase in current from a photomultiplier tube coupled with ZnS screen because of the incidence of the alpha particle. In 1947-48 Marshall and co-workers designed a photomultiplier scintillation detector with a well-designed optical system to reflect the scintillation emission on the photocathode. Broser and Kallmann (1947) discovered ZnS, $CaWO_4$, $ZnSO_4$ and naphthalene scintillator capable of detecting beta and gamma radiations. The development of photomultiplier tube led to the development of various kinds of scintillator detectors. Bell (1948) discovered that crystalline anthracene has five times better scintillation amplitude and, thus, is more suitable than naphthalene. Collins (1948) measured the scintillation decay times of anthracene and naphthalene and observed it ~ 10^{-8} s, indicating better resolving time than any gas ionization counter. Hofstadter (1948) discovered that NaI(Tl) shows larger scintillation pulses than anthracene and attributed the same to the high photoelectric absorption. This is used for spectroscopy of gamma sources. There were other developments in the field of organic scintillators in 1949-50. Ageno et al. (1949, 50), Reynolds et al. (1950) and Kallmann (1950) found that certain organic liquids exhibit scintillation

comparable to the anthracene crystals. Schorr and Torney (1950) discovered similar behavior in organic plastic solutions. Further, Birks (1950) observed increased scintillation efficiency by dissolving a small quantity of anthracene in a naphthalene crystal. The liquid, plastic and crystal solution scintillators each exhibit scintillation by efficiently transferring of ionizing radiation excitation energy from the solvent to the solute, emitting its characteristic fluorescence. The decay time of liquid and plastic organic scintillator is ~2-3 ns, higher than the organic crystals and their easy preparation in large volumes has led to the realization of wide-scale utilization. (Flakus, 1981)

2.5 Mechanism of Radiation Sensing

As explained in earlier sections, the interaction of radiation with medium leads to the creation of electron-hole or ion pairs. These generated electron-hole pairs carry the information of radiation absorption. Thus, either direct collection/measurement or other effects produced by these charge carriers can be used to correlate with radiation absorptions. Radiation can be detected in (i) active mode, i.e., real-time detection of radiation is carried out by immediate effects produced by absorption or (ii) passive ways, where charge carriers are trapped at some center in the material and then released by stimulation such as heat, light or electric filed. Generally, four mechanisms are adopted for radiation detection and measurement, as discussed in the following sub-sections.

2.5.1 Ionization Detector

Ionization detectors utilize a medium with which radiation interacts, generating electron and hole/ion pairs (figure 2.15 a) and electric field across the medium to collect these charge carriers. The current /voltage signal generated at one terminal fed to the preamplifier for amplifying the signal to the sufficient level required for further processing. The preamplifier signal is then shaped and further amplified before counting or multichannel analysis (Figure 2.15b)

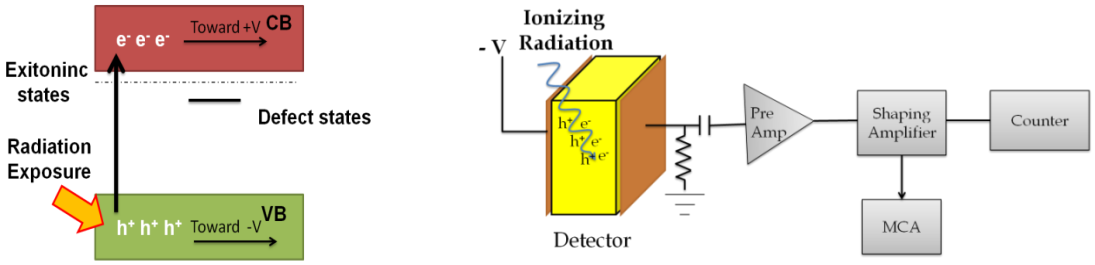

Figure 2.15: (a) Band Diagram schematic showing the ionization process (b) Schematic design of ionization detector

The interacting medium can be solid or gas. The gas detectors such as ionization chamber, proportional counter and GM Tubes work on such principle. Solid-state detectors are basically semiconductor detectors such as Si, Ge and Cadmium Zinc Telluride (CZT), which are widely used in radiation spectroscopy. Such semiconductor devices can be used in two modes: (i) pulse mode for spectroscopic applications and (ii) photoconductive mode for dosimetry application.

In a spectroscopy detector, a high electric field is applied on two opposite faces of semiconductor material (figure 2.16.) Here, ionizing radiation interacts within the semiconductor medium of thickness W and results in electron-hole pairs. These carriers sweep across the device to opposite polarity electrodes. An induced charge, crated at the terminal due

to charge carrier movement in the semiconductor, depends on the distance traveled by charge carrier.

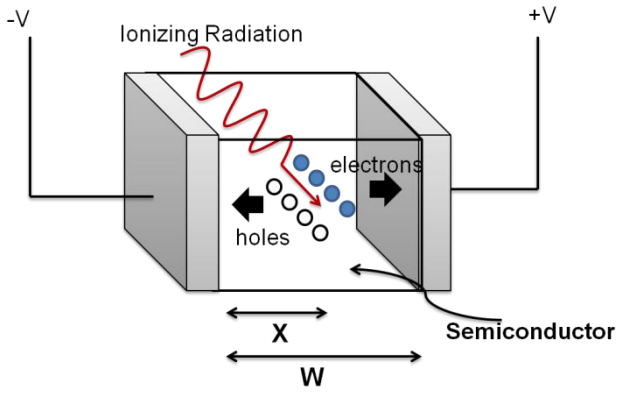

Figure 2.16: Ionization Radiation-induced creation e-h pairs and collection by an electric field (Knoll, 2010; McGregor and Hermon, 1997)

The induced charge dQ* at the terminal due to N_0 electron-hole pair traveling a distance dx in the semiconductor of thickness W is given as;

$$dQ^* = \frac{qN_0}{W}dx$$

This relation is valid for an ideal semiconductor, i.e., semiconductor with no defects. In a real semiconductor, defects are present and affect the charge carrier's movement within the medium. Thus, the induced charge for a semiconductor with defects is different from the ideal case and is given as;

$$Q^* = qN_0\left[\frac{v_h\tau_h^*}{W}\left(1 - exp\left[\frac{-x}{v_h\tau_h^*}\right]\right) + \frac{v_e\tau_e^*}{W}\left(1 - exp\left[\frac{(x-W)}{v_h\tau_e^*}\right]\right)\right]$$

v_h and v_e are respective carrier drift velocities, $\tau_h^*$and τ_e^* are mean drift time for holes and electron, respectively and x is interaction location (figure 2.16). The spectroscopic resolution is determined by the mean free time for either charge carrier. The resolution of a detector is determined by the carrier extraction factor $\frac{v\tau}{W}$ and is considered degraded if $\frac{v\tau}{W}$< 50 (Knoll, 2010; McGregor and Hermon, 1997).

A photoconductive mode is used for radiation measurements, where spectroscopic information is not required/ essential. A photoconductive semiconductor detector consists of two ohmic contacts on the opposite surfaces of the semiconductor. A current is produced by free charge carriers in the absence of ionizing radiation and is known as equilibrium current or background current, which is measured by applying a voltage on these contacts. The exposure of ionizing radiation to the detector significantly increases the current above the equilibrium current and is known as photo-current. The photo-conductive gain of the detector is given as(Knoll, 2010)

$$G = \frac{\mu_c\tau_c^*\mathcal{E}}{W} = \frac{\tau_c^*}{t_c}$$

where μ_c is the charge carrier mobility, τ_c^* is the carrier lifetime, t_c is the carrier drift time across the detector, $\mathcal{E}$ is applied electric field and $W$is the detector thickness.

2.5.2 Radiation-Induced Scintillation

Scintillators are certain materials that emit UV-Vis light pulse on exciting with ionizing radiation. In this mechanism, radiation induced created electron-hole recombination result in a prompt emission of UV-vis light called radiation-induced scintillation or radioluminescence,

which can be measured with a photon detector (figure 2.17). There can be two different way of recombination one through exitonic transitions which are very fast with decay time ~ ns and other through the defect states which are relatively slower having decay time ~ μs.

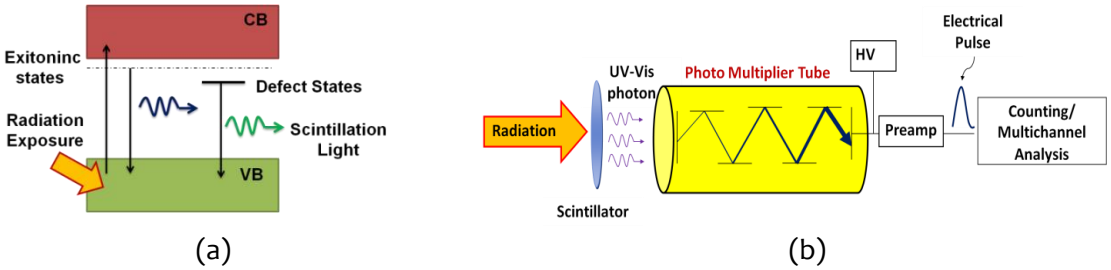

Figure 2.17: (a) Band Diagram schematic showing the scintillation process (b) Schematic design of scintillator detector

A scintillator is characterized by the physical and luminescence characteristics of the material. An ideal scintillation should have physical characteristics such as high density, chemically and mechanically stable and radiation hard, particularly for scintillators, used in high energy experiments together with low development cost. Luminescence characteristics such as high light yield and emission wavelength should match a photodetector's peak spectral response such as PMT and photodiode. The average energy for the creation of one e-h pair should be proportional to that of recoiled electron for good resolution and fast luminescence decay time. PbI_2, CdS and ZnO are some of the important semiconductor scintillator materials (Derenzo et al., 2003).

Interaction of ionizing radiation with scintillator materials results in photons in three-stage processes, i.e., creation of hot electron pairs, thermalization and transport to luminescence center. The number of photons generated during the process will depend on the number of electron-hole pairs $N_{e\text{-}h}$ produced during the process, transfer of electron-hole pair energy to luminescence center (S) and quantum yield of the luminescence process (Q) (Rodnyi et al., 1995).

$$N_p = N_{eh} SQ$$

The number of electron-hole pairs generated is determined by the energy deposited in the medium (E_R) by radiation and average energy for the creation of electron-hole pair E_{eh}.

$$N_p = \frac{E_R}{E_{eh}} SQ = \frac{YE_R}{E_g} SQ$$

Where $Y=E_g/E_{eh}$ is termed as relative yield of electron-hole pair. If N_p photons are created with average energy $h\nu_m$; ν_m being the frequency of the maximum emission per unit absorbed energy E_R then energy efficiency ϱ is expressed as;

$$\boldsymbol{\varrho = \frac{N_p < h\nu_m >}{E_R} = Y \frac{< h\nu_m >}{E_g} SQ}$$

This shows that higher scintillation efficiency can be achieved with lower bandgap material. Another important property of the scintillator is scintillation decay time, affecting efficiency.

2.5.3 Stimulated Luminescence Measurement

This is a passive method for measuring ionizing radiation doses, consisting of emission of light due to thermal/optical stimulation of pre irradiated samples. The traps within the material capture electron-hole pairs, produced due to the radiation. The heating/optical stimulation of such exposed materials results in the emission of UV-Vis photons, which are sensed/collected by a PMT (figure 2.18). The amount of light produced is plotted versus the

temperature variation, known as the "Glow Curve," consisting of one or multiple peaks, thus showing the materials' TSL characteristics.

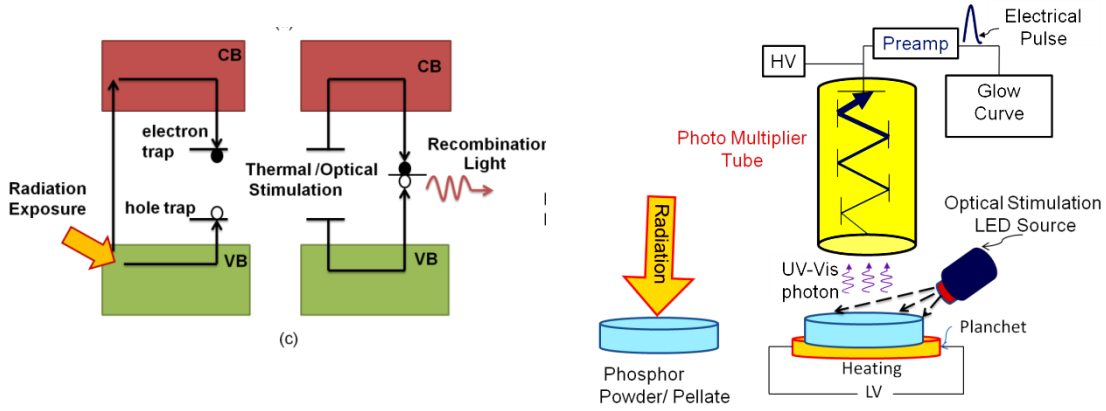

Figure 2.18:(a) Band Diagram schematic showing the thermal/optical in stimulation (b) Schematic design of scintillator detector

A thermoluminescent material is characterized by luminescence characteristics such as (i) a simple glow curve peak at high temperatures, (ii) emitting light wavelength, which should match to the PMT's spectral response, (iii) good charge storage stability (low fading), (iv) tissue equivalent material for personal dosimetry, linear with radiation dose, (v) independent of radiation dose rate and (vi) non-toxicity of the material (Furretta, 2003).

Considering one trap and one recombination centre (Sunta, 2015), the intensity of emitted light at time t depends on the number of trapped electron density 'n' and probability of de-trapping 'p' as;

$$\boldsymbol{I(t) = np}$$

The probability of de-trapping at temperature T from a trap at trap depth E from conduction band is given as = $\boldsymbol{se^{-E/kT}}$, where 's' is the attempt to escape frequency. Thus, the intensity of emitted light becomes

$$\boldsymbol{I(t) = nse^{-E/kT}}$$

The variations of n, p and n*p are plotted with temperature T in figure 2.19. The trapped charge carriers are maximum at room temperature due to radiation exposure. When the material is heated with a linear temperature profile ($T=T_0+\beta T$, β heating rate), the trapped charge carrier starts de-trapping from their traps and recombine with the hole to generate light. As the temperature increases, the probability of de-trapping increases. The multiplication of these two parameters, i.e., 'n*p' provides a glow curve, which exhibits a peak at a specific temperature.

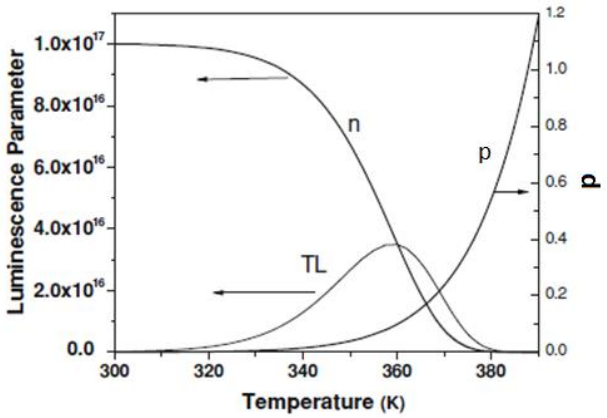

Figure 2.19: Plot of trapped electron n, probability p and Intensity of Glow curve np (Sunta, 2015)

The trap centers in a TL material are basically defects that may be intrinsic or introduced by doping certain impurities. The defects at various depths from the conduction band result in the glow curves with multiple peaks, where each peak will correspond to the respective defect states.

Instead of thermal stimulation, the traps can also be emptied by optical stimulation as well and the phenomenon is known as optically stimulated luminescence (OSL). There are three-way of using light stimulation: (i) Continuous wave mode (CW-OSL), where steady illumination with light of wavelength λ and fixed intensity Φ is used, (ii) Linear Modulation (LM-OSL) mode, where the sample is illuminated with intensity linearly varying with time $\Phi(t)=\Phi_0+\beta t$, where $\beta=d\Phi(t)/dt$ and (iii) Pulsed mode (P-OSL) where a pulsed illumination is given to the sample with intensity $\Phi(t)=\Phi_0$ for $t_0 \leq t < t_0+\Delta t$ and $\Phi(t)=0$ for $t_0+\Delta t \leq t < t_0+\tau$; τ is the period of the pulse(Botter-Jensen et al., 2003).

In the simplest model with one trap center and one recombination center, the OSL curve obtained in continuous-wave stimulation is exponential decay curve (figure 2.20 a) and the OSL signal is given as $I_{OSL} = I_0 exp\,(-\frac{t}{\tau_d})$, where τ_d is the decay constant for CW-OSL, I_0 is OSL intensity at t=0. However, a significant deviation from the above equation is observed for the case of multiple traps.

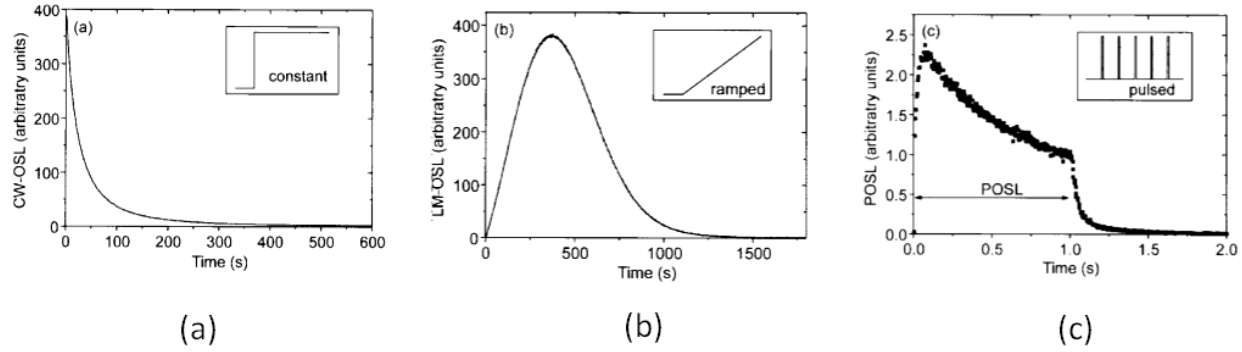

Figure 2.20: OSL curve in three stimulation scheme (a) Continuous-wave OSL (CW-OSL) (b) Linearly Modulated OSL (LM-OSL) and (c) Pulsed OSL (P-OSL) (Botter-Jensen et al., 2003))

In the case of LM- OSL, the ramped light flux $\Phi(t)=\gamma t$ is used for stimulation. The intensity of the OSL curve is given as

$$I_{LM-OSL} = n_0 \sigma \gamma t exp\left\{-\frac{\sigma\gamma}{2}t^2\right\};$$

Where n_0 is the concentration of electron in trap at t=0, σ is photoionization cross-section probability γ is ramp rate. OSL curve obtained in LM mode is shown in figure 2.20 b.

Similarly, in the case of P-OSL, the intensity of OSL for pulse duration Δt (Yukihara and McKeever, 2011),

$$I_{POSL} = \frac{m^*(\Delta t)}{\tau} exp\left(-\frac{t}{\tau}\right)$$

where $m^*(\Delta t)$ is the concentration of excited centers. OSL curve obtained in POSL mode is shown in figure 2.20 c.

2.5.4 Radiation-Induced Change in Optical/Electrical/Structural Properties

This method includes the creation of point defects such as vacancies or interstitials after exposure to the high dose of ionizing radiation and thus, change in optical properties such as bandgap, absorbance, etc.; electrical properties such as conductivity and capacitance; and structural properties such as crystallinity which can be estimated using respective characterization tools (figure 2.21)

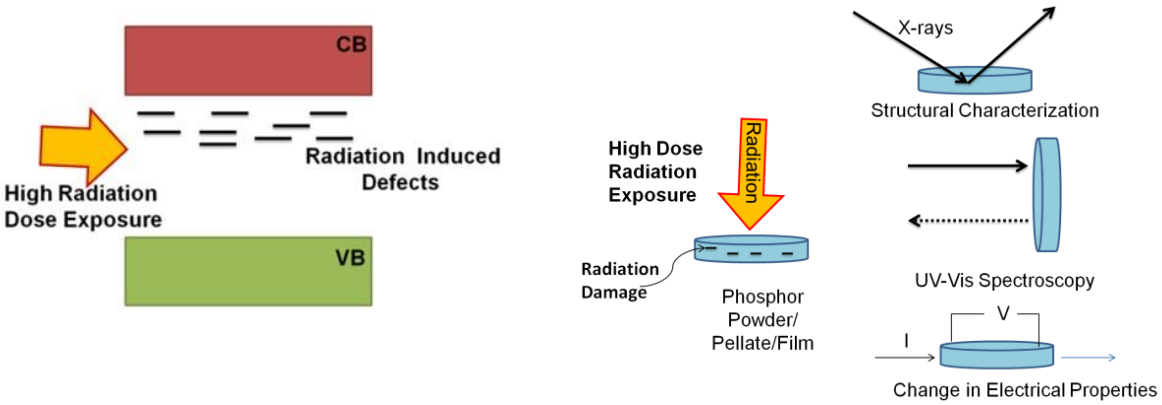

Figure 2.21:(a) Band Diagram schematic showing the Radiation-induced effects (b) Schematic of characterization for measurement of effects

High radiation dose exposure to semiconductor materials results in significant changes in their physical properties, such as optical, electrical and structural properties. It is useful in estimating the exposure quantity. The change in electronic properties may vary the bandgap of material, which is described by the relation (Mott and Davis, 1979);

$$\alpha h\nu = B\,(h\nu - E_g)^n$$

Where α is absorption coefficient, B is a constant and E_g is band gap, n=1/2 for direct transitions and 2 for indirect transitions. The absorption coefficient α is related to ΔE, the width of localized state band tails given Urbach rule

$$\alpha = \alpha_0\, exp\left(\frac{h\nu}{\Delta E}\right)$$

After radiation exposure, the localized states are created, ΔE increases and thus, changes α and the bandgap. The change in bandgap leads to the corresponding change in conductivity and capacitance. The electrical conductivity is given as $\sigma = \frac{It}{VA}$; where I is current, t is the thickness of the sample, V is the applied voltage and A is the area of the sample. It is related with bandgap and temperature with Arrhenius relation as;

$$\sigma = \sigma_0\, exp\left(-\frac{E_g}{\mathrm{kT}}\right)$$

Thus, an increase in ΔE decreases the bandgap after radiation exposure, which finally increases the conductivity.

Apart from optical and electrical properties, structural properties of the detector material such as crystallinity, grain size, strain are also modified after radiation exposure. These properties can be measured using X-ray diffraction experiments.

2.6 Synthesis Techniques for Detector Materials for Ionizing Radiation Detection

Ionizing radiation detector material consists of various structures such as bulk single crystal, thin/thick film, transparent ceramics, powder used as a medium for interaction with ionizing radiation and produces some measurable effects. These sensor materials can be developed by different methods, as described in following subsections.

2.6.1 Bridgman and Hydrothermal Method

The Bridgman method, developed in 1925 is used to develop various single-crystal detectors(Bridgman, 1925). It is fast and relatively simple as compared to other single crystal

growth methods. It consists of quartz ampoule for melting the material with neck to facilitate nucleation and gradually move the melt from a hot zone to a cool zone with a fixed temperature gradient. Nucleation at the tip of the ampoule occurs as it comes in a cool zone which acts as a seed for the growth of entire melt in a single crystal. The quality of the crystal is determined by the speed of the ampoule moving in the hot zone. NaI(Tl), CsI(Tl), CsI(Na), $LaBr_3$:Ce scintillators for gamma radiation spectroscopy are grown by Bridgman method (Hofstadter, 1949). ZnO, ZnO:Ga and ZnO doped with other dopants were developed using the modified Bridgeman method.

The hydrothermal method utilizes the high temperature/pressure properties of water, which dissolves materials not soluble in ordinary conditions, to make a crystal. The process was developed in 1845 by for development of quartz crystal. This process is responsible for natural formation of mineral in earth crust. In Laboratory, this process is performed on platinum lined vessel called Morre's Vessel or autoclave filled with water /mineraliser and nutrients and kept at temperature ~200-300 ^{0}C and several kbar pressures. Various oxide materials $BaTiO_3$, ZnO, Fe_2O_3, ZrO_2, TiO_2, Al_2O_3, zeolites and Quartz are developed using this method. High purity ZnO single crystal developed using this method for detection of alpha particles and X rays.

2.6.2 Uniaxial Hot Press and Spark Plasma Sintering (SPS)

Sintering of polycrystalline material for prolong time results in slightly increased transparency. Highly transparent ceramic scintillators are obtained using pressure-assisted sintering in which powder is heated at a high temperature ~1000 ^{0}C or with simultaneous application of pressure. Uniaxial Hot pressing and Spark Plasma Sintering, also known as Field Assisted Sintering (FAST), are two popular methods of fabricating transparent ceramic scintillators. In the Uniaxial Hot pressing method, the powder material is subjected to high pressure and temperature, increasing grains and transparency (figure 2.22a) (Chernenko et al., 2018). SPS is a versatile process for obtaining dense transparent ceramics with fine grains. The powder is placed in a conductive graphite die and ~100 MPa pressure is applied in conjunction with a high direct current is passed, resulting in rapid heating of the powder converting into ceramic (figure 2.22 b). SPS is used for the preparation of various oxide transparent ceramics such as Al_2O_3, SiO_2, Y_2O_3, Lu_2O_3 and Others (Futami et al., 2013; Neal et al., 2009)

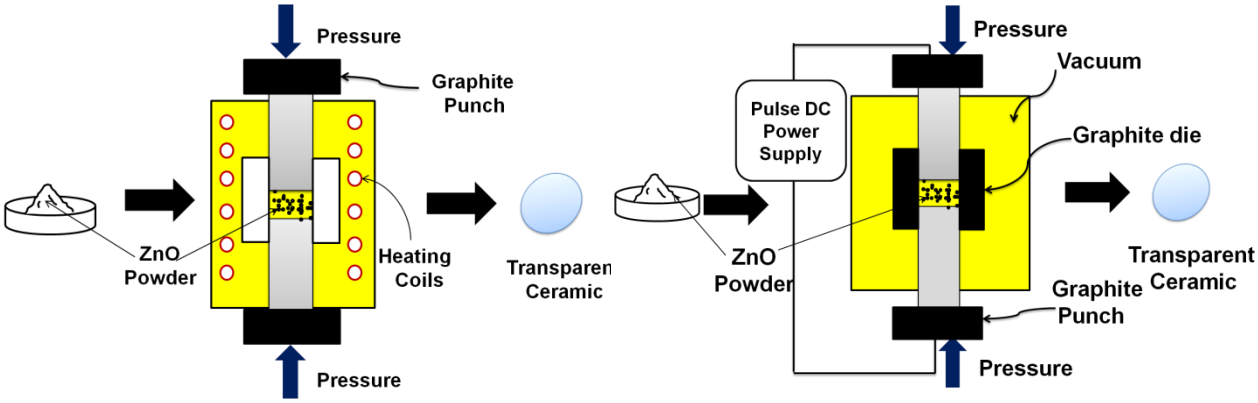

Figure 2.22: Uniaxial hot pressing and Spark Plasma Sintering

2.6.3 Liquid Phase epitaxy

Liquid phase epitaxy (LPE) is a method of growing thin film at high temperatures initially introduced in 1963(Nelson, 1974). This method is used to grow III-V, II-VI and IV-VI compounds such as GaAs, GaP, AlGaAs, magnetic garnets and others (Kuphal, 1991). It is used

for growing the epitaxial layer of the desired material on a suitable substrate by contacting at high temperatures. It is done in three ways: (i) tipping, (ii) dipping and (iii) sliding boat. In the tipping process, melt and substrate are kept at the opposite ends of a tilted boat made of silica or graphite. The furnace is tipped to facilitate the rolling of melt over substrate and resumed back to its original position resulting in the growth of the epitaxial layer on the substrate. A substrate is dipped in melt and rotated for uniform growth of epitaxial layer in the dipping process. The sliding boat method is used for multilayer epitaxial growth in which melt and substrate made in contact using a sliding mechanism (Capper et al., 2017). LPE method is used to grow various thin film single crystalline oxide scintillators using fluxes such as PbO, PbF_2, BaO, B_2O_3, Bi_2O_3, MoO_3 (Kucera and Prusa, 2017). LPE grown LSO:Tb thin-film scintillator is reported for X-ray imaging application (Cecilia et al., 2011). $Tb_3Al_5O_{12}$:Ce, ZnO:In and ZnO:Mg scintillation screens are also reported for alpha particle detection (Sekiwa et al., 2010; Yoshikawa et al., 2012; Zorenko et al., 2017)

2.6.4 Sol-Gel Method

The sol-gel method is used to prepare nanoparticles that can either be directly used for luminescence dosimetry application or embedded in a transparent polymer matrix resulting in a nano-composite scintillator. The sol-gel method consists of the dissolution of metal-organic compounds in a suitable solvent such as alcohol or water, resulting in the formation of colloidal solution due to hydrolysis followed by elimination of alcohol/water by forming gel due to condensation process. The calcination of gel results in the formation of metal oxide nanoparticles. Various metal oxide nanoparticles, e.g., ZnO, TiO_2, SnO_2, WO_3, are prepared using this method (Parashar et al., 2020). The sol-gel method is used to prepare nanoparticles, which act as an absorber for X-ray(Sun et al., 2014) and neutrons scintillator(Im et al., 2004). Rare-earth doped Gd_2O_3 and Lu_2O_3 prepared by sol-gel route have been investigated for the development of X-rays scintillator(Garcia-Murillo et al., 2003).

2.6.5 Sputtering

Sputtering is one of the physical vapor deposition methods of thin films, consist of a target material, for sputtering using energetic ions. Target is kept at negative potential under vacuum. Ions of inert gas such as Argon is used to eject target atom which deposits on silicon or other substrate producing a thin film. A flexible X-ray radiation dosimeter is reported using RF magnetron sputtering grown amorphous Ga_2O_3 thin film developed (Liang et al., 2019). It consists of amorphous Ga_2O3 deposited on polyethylene nepthalate (PEN) substrate with interdigitate electrodes. Photocurrent measured under X-rays exposure shows that the film is sensitive to X-rays. CdTe sputtered thin film on Molybdenum (Mo) substrate is reported as X-ray/Gamma radiation sensor. The measured energy resolution ~5 keV for ^{241}Am (59.6 keV) gamma radiation(Zaveryukhin et al., 2003). Flexible metal oxide transistor consisting Indium-Gallium-Zinc Oxide (IGZO) as semiconductor and multilayer dielectric materials such as SiO_2 and Ta_2O_5 is used for X-ray dosimeter (Cramer et al., 2018). Magnetron sputtering is used for the production of ZnO:Ga scintillation film, which has application in the detection of pulsed X-rays, protons and alpha particles (Wen et al., 2019)

2.6.6 Solution Combustion Synthesis (SCS)

The solution combustion method consists of exothermic reaction in aqueous or sol-gel media, which is self-sustained. This process is used for the preparation of nanoparticles (Varma et al., 2016). It is an auto-ignition process mediated by fuels such as glycine, citric acid, urea, ascorbic acid, etc. Various rare earth oxides such as Eu_2O_3, Gd_2O_3 and Dy_2O_3 are prepared using this method (Tyagi, 2007). Binary metal oxides such as ZnO, TiO_2, Fe_2O_3, WO_3, SnO_2, ZrO_2, Perovskite Oxides and other complex oxides are prepared using SCS are useful for energy storage and conversion applications (Li et al., 2015). Undoped and Fe doped ZnO nanoparticles prepared by SCS method have shown the application in thermoluminescence dosimetry for

gamma radiation (Jagannatha Reddy et al., 2011; Reddy et al., 2012) and beta radiation (Orante-Barrón et al., 2015; Pal et al., 2006).

2.6.7 Co-Precipitation

It is a process in which two or more compounds precipitate from a solvent. Oxide, Fluoride and oxyfluoride nano phosphor were prepared using this method. Water/ Ethanol soluble precursor such as nitrate, chloride, or acetate is used to make solution in the desired solvent. A precipitating agent is added dropwise resulting in the precipitation of desired compound (Tyagi, 2007). This method is utilized for the preparation of thermoluminescent/optically stimulated luminescent materials. $CaSO_4$:Dy (Rivera et al., 2010), CaF_2:Mn (Palmer et al., 1965), $LiPO_3$:Tb^{+3} (Palan et al., 2016) etc. for beta and gamma radiation. Ceramic powder scintillator such as $Gd_3Ga_3Al_3O_{12}$:Ce (Sen et al., 2017), Lu_2O_3 and LuAG:Ce (Tret'yak et al., 2015) and other ceramic scintillator were obtained using this method. The TiO_2 nanoparticles, prepared using the co-precipitation method, are used for thermoluminescence dosimetry of gamma radiation dose, ranging from few Gy to kGy (Azorín-Vega et al., 2007; Sharmila et al., 2019). ZnO nanoparticle obtained using this method has reported beta TL/OSL properties (Soares et al., 2017).

2.6.8 Solid-State Reaction

The solid-state reaction employs the diffusion of two or more solids at high temperatures for the synthesis of polycrystalline materials. Solid reagents are mixed in stoichiometric ratio and subjected to a high temperature in the furnace under different air, vacuum, nitrogen or inert environments. Tamman's Rule determines the temperature, i.e., the minimum temperature should be two-third of the meting point of the lowest melting reactant. Various metal oxides, sulfide, silicates and nitrides are prepared using this method. Various scintillators such as ZnS:Ag(Wu et al., 2019), GdOBr:Ce (GOB), SrI_2:Eu, CaI_2:Eu (Fiserova and Janda, 2018), ZnO:Ga (Bourret-Courchesne et al., 2009) are prepared using this method for alpha and neutron detection applications. Several phosphor such as ZrO_2:Eu (Tamrakar et al., 2014b), Y_2O_3 (Dubey et al., 2015), $Zn(BO_2)_2$:Tb (Li et al., 2007), Y_2SiO5:Eu^{+3} (Parganiha et al., 2015), $BaSO_4$:Eu (Annalakshmi et al., 2012), Gd_2O_3: Er^{+3} (Tamrakar et al., 2014a) prepared using solid state method are reported for thermoluminescence dosimetry applications.

2.6.9 Hydrothermal method

The hydrothermal method involves the dissolution of reactants under room temperature or high temperature and environmental or elevated pressure conditions. This process is used to fabricate nanostructures such as nanoparticles, nanorods, nanowires, etc. (Gan et al., 2020). The hydrothermal reaction is performed in an autoclave which can sustain high temperature and pressure. Metal oxide nanoparticle is prepared in supercritical water. Metal nitrate solution is dissolved in water to get hydrolyzed from metal hydroxide (M-OH), followed by dehydration, resulting in precipitation in the form of metal oxide. ZnO, TiO_2, SnO_2, $BaTiO_3$, Fe_2O_3, CeO_2 and other metal oxide nanoparticles can be prepared using this method (Hayashi and Hakuta, 2010). For ZnO nanorods, the substrate is seeded with ZnO seeds and ZnO nanorods are grown by keeping substrate in ZnO aqueous solution at 90^0C (Yang et al., 2009).

2.6.10 Method for Composite Preparation

Composite materials, a mixture of two or more materials, are a cost-effective alternative to single crystals or transparent ceramic detectors. The polymers, such as PMMA, Polystyrene (PS) and others, are used as base materials in which a scintillator material is dispersed. Thin scintillator film is casted for measurement of X-rays, alpha particles, etc. Inorganic nanoparticles of Gd_2O_3:Eu^{3+}, $Y_2Hf_2O_7$:Eu^{3+}, $Gd_3Ga_3Al_2O_{12}$:Ce (GGAG) embedded polymer composite reported

for X-ray imaging application (Koshimizu, 2020). Composites can be prepared using three methods:
(1) Mixing the scintillator in monomer or polymer base mixed with hardener followed by polymerization or curing to obtain a composite scintillator. This process is reported to prepare stilbene/organosilicon polymer composite for neutron detection (Lee et al., 2014)
(2) A mixture of scintillator and polymer granules is pressed using stainless steel slabs. ZnO:Ga/Polystyrene composite scintillator for X-ray measurements (Burešová et al., 2016)
(3) Polymer granules dissolved in a solvent to make transparent solution and addition of scintillator material followed by drying. Preparation of CeF_3 and BaF_2 based composites are reported using this method (Demkiv et al., 2016, 2018).

2.7 Zinc Oxide as Ionizing Radiation Detector and Dosimeter

Zinc oxide (ZnO) is a wide band semiconductor. Over the decades, it has been explored because of its numerous applications such as piezoelectric transducers, optical waveguides, acousto-optic media, conductive gas sensors, transparent conductive electrodes, etc. Zinc oxide semiconductor commonly crystallizes in wurtzite structure which may change to zinc blend by applying high pressure. In the wurtzite structure, each Zn atom is surrounded by four O atoms in tetrahedral configuration and vice-versa. Also, the terminating face (0001) in Zn face and (000-1) O face are the polar faces and responsible for piezoelectric behavior in ZnO (figure 2.23a) (Heiland et al., 1959; Heiland and Kunstmann, 1969). The sp^3 hybridization causes the direct bandgap formation in ZnO. The sp^3 bonding constitutes the valence band whereas anti-bonding constitutes the conduction band. ZnO's large room-temperature band gap is 3.37 eV, which is in the UV region of EM spectrum, making it suitable for several optical applications. The room temperature photoluminescence (PL) of ZnO consists of a sharp peak near 3.4 eV, called near band edge emission (NBE) and a broad peak near 2.45 eV, which is attributed to the intrinsic defects such as oxygen vacancies, called Defect Band Emission (DBE) (figure 2.23 b) (Børseth et al., 2006; Leiter et al., 2001; Rodnyi and Khodyuk, 2011; Vanheusden et al., 1996)

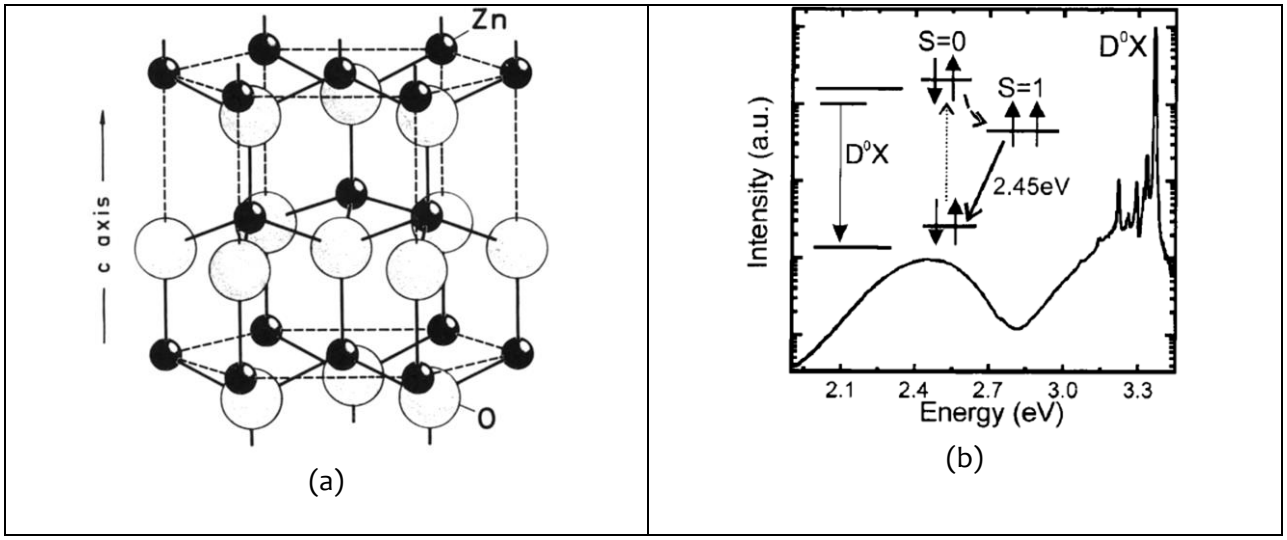

Figure 2.23: Structure and Photoluminescence of ZnO (a) Wurtzite Structure of ZnO Crystal (G. Heiland and P. Kunstmann, Surf. Sci. 13, 72 (1969) (b) Photoluminescence of ZnO at 5K excited by HeCd laser (Leiter et al., 2001)

The scintillating properties of ZnO are investigated since 1960s (Lehmann, 1966). In the 1960s, Lehmann explored the use of Ga doped ZnO powder for scintillation applications. However, the reported luminescence is poor because of the powder nature of the material. With the recent advances in crystal growth technology, ZnO scintillation properties can be dramatically improved by producing large diameter single crystals or large single crystal thin films. The luminescence decay time of NBE is of the order of nanosecond because of the

excitonic decays, whereas defect luminescence decay times are large compared to NBE. The defect luminescence is avoided for such applications, where a fast response is required. This can be done either by annealing of ZnO in a reducing environment or doping of n-type impurity in ZnO such as Ga (Lehmann, 1965, 1966). ZnO is widely used as a scintillator for X-ray imaging and detection of alpha particles and gamma rays because of its suitable intrinsic luminescence and scintillation characteristics. ZnO scintillator detector in combination with neutron converter materials such as Boron-10 or Lithium-6 may also work as a detector for thermal neutrons. ZnO single crystal based scintillators are developed for detection of alpha particle detection and are commercially available as ionization detector. Zinc oxide single crystal and thick films can be used for measurement of X-ray/gamma radiation doses as ionization detector. High resistivity ZnO crystal with metal contacts on opposite faces acts as a radiation detector for X-ray dose rates from few mGy/s to Gy/s. ZnO luminescent powder-coated transparent substrates are used for making a scintillation screen. Powder scintillator layer thickness is limited as the transparency reduces drastically with the thickness of the scintillator. When subjected to high temperature ~1000^{0}C and pressure 15-20 MPa, these powder materials are converted into transparent ceramic, allowing the scintillation light to pass through it. Hot pressing and Spark Plasma sintering are two methods commonly used for preparing transparent ceramics of undoped and doped (with certain activator) zinc oxide. Another way of using a powder scintillator is nano-composites, a mixture of organic host matrix and nanoparticles of scintillating material. The scintillation mechanism in this type of scintillator utilizes the Forster energy transfer (FRET) process. In FRET, the radiation energy is absorbed by the organic molecule and then transferred to the scintillating material. ZnO nanocomposite scintillators are used in alpha, gamma and neutron detection. ZnO thin film detectors in combination with neutron converter materials have shown potential for the neutron radiation detector.

ZnO thick films, made with a polymer binder, show change in I-V characteristics in reverse bias due to damage created by the radiation. Interdigitated electrodes on such film facilitate online measurement of change in capacitance due to radiation exposure. While Scintillator and Ionization-based detectors offer online radiation measurement, undoped and doped ZnO powder/pellets exhibit thermoluminescence/ optically stimulated luminescence when exposed to ionizing radiation, making it a suitable radiation dosimeter. Intrinsic defects in ZnO may have different energy positions from the conduction band. Therefore, exposure of beta/gamma radiation to ZnO material leads to the capture of electrons and holes at these traps. Thermal stimulations result in the release of these trapped charge carriers and subsequent recombination. Thus, luminescence glows show multiple peaks ranging from 130 to 450 ^{0}C. Apart from intrinsic defects, intentional doping may also change in the glow curve and other TL properties.

High exposure of several kGy leads to changes in physical properties such as structure, optical and electronic properties, which can be measured using X-ray diffraction, optical characterization and electrical measurements, respectively. Gamma exposure results in Zn metal formation, showing the onset of (100) peak associated with Zn in ZnO nanowire exposed to 100 kGy. Oxygen vacancies created by gamma exposure results in reduced transmittance and bandgap. Table 2.6 summarizes the different structures of ZnO and detector types used for the detection and measurement of ionizing radiation.

2.8 Synthesis and Characterization of Zinc Oxide Structure for Ionizing Radiation Detection and Measurement

2.8.1 Single Crystal Detectors

Zinc Oxide single crystal has been reported mostly as a scintillator and ionization detector for pulsed radiation detection. Fast response is one of the desirable features of any scintillator. However, the defect luminescence of ZnO makes its response relatively slow. Ga doping is one of the earliest ways to minimize the effects (Lehmann, 1966). Ga^{3+} donate a free electron that suppresses the defect luminescence in ZnO. Only near-band-edge emission is observed, making it a fast scintillator with a decay time of the order of a few ns. Many developments are reported on the synthesis of doped and undoped zinc oxide material. Single crystals of doped and undoped ZnO are developed using various techniques such as hydrothermal, direct high-pressure melting, vapor phase epitaxial method, chemical vapor transport and molten salt method (Huang et al., 2014). A high-quality scintillator for detecting alpha radiation has been reported using the first two methods (Neal et al., 2008; Yanagida et al., 2010). Nause et al., 2005 developed a method for fabrication of ZnO single crystal using pressure melt method where ZnO is melted in the presence of oxygen pressure to fill oxygen deficiency produced during melt of ZnO. Modified Bridgman apparatus is used for the preparation of pressure melt ZnO single crystal. ZnO is melted using joule heating induced by radio-frequency under a pressurized oxygen environment at 1-100 atm pressure. A two-inch diameter circular, highly pure ZnO crystal is grown. The photoluminescence of the developed crystal showed NBE and defect luminescence (Nause and Nemeth, 2005). Using this method, Cermet Inc, USA(Rengarajan et al., 2007) developed ZnO single crystal doped with various impurities such as Li, Gd, Ga, Er & Li, Mg , Ga & Li. The developed crystals are evaluated for alpha radiation detection. The pulse height response with alpha radiation detector studied and showed that ZnO, ZnO:Ga, ZnO:In,Li and ZnO: Er,Li show fast decay less than 10 ns, whereas ZnO:Ga, ZnO:Li and ZnO: Mg,Ga show slow decay greater than 1μs (Neal et al., 2008).

Another method for ZnO single crystal growth is the hydrothermal method which utilizes supercritical water at a temperature ~400 ^{0}C and pressure of 80-90 MPa to grow ZnO single crystal (Maeda et al., 2005). Reactions were performed in Pt-lined autoclave with two different temperature zones. ZnO is dissolved in a mixture of concentrated alkali hydroxide (LiOH+KOH) and kept in the high-temperature zone. ZnO crystal grows on a seed crystal, kept in the low-temperature zone. X-ray and PL characterizations show the high crystallinity and intense luminescence peak at 3.37 eV compared to lower energy defect band PL shown by highly pure ZnO crystals. ZnO grown 2-inch crystal using the hydrothermal method is demonstrated for efficient alpha imaging applications (Yanagida et al., 2010) by coupling it to a position-sensitive photomultiplier tube (PSPMT) in conjunction with a counting readout circuit. Alpha excited pulse height spectrum is studied and integrating whole event, a resultant 2D image is created. The image consists of noise fragments that are removed by integrating selected channels of pulse height spectrum from 500-1000. The image obtained is free from noise fragments.

Another single crystal of ZnO doped with scandium is developed using a hydrothermal method at 0.1-0.3 mol% concentration of scandium (Zuo et al., 2011). The variation in scandium concentration results in the formation of ZnO:Sc crystal in different directions. As the concentration increases to 0.3 mol%, the crystal develops along the (0001) direction. X-ray characterization shows (0002) reflection, whereas the photoluminescence spectrum shows a sharp peak at 377 nm and a broad peak at 556 nm. Using the same method 15 mm x 15 mm x 3 mm ZnO:Sc crystals are developed and used for scintillation application as sub-nanosecond pulsed radiation (Zhang et al., 2014). Alpha excited pulse height spectrum using Ga and Sc

doped ZnO suggests that ZnO:Sc has wider spectrum with lower intensity than that of ZnO:Ga. Alpha exciting time response for ZnO:Sc crystal studied and rise time of 162-170 ps and fall time of 300-329 ps are noticed, which are very suitable for its application as sub nano pulsed radiation detection.

Hydrothermally grown highly resistivity ZnO substrates are also utilized as X-ray radiation sensors (Endo et al., 2011). The sensor was designed by using Pt electrode on Zn Face and AZO film. Titanium and gold films of different thicknesses are deposited on opposite O-face using magnetron sputtering and packaged in the form of a chip. The sensor with biasing at 20 V is exposed to X-rays and operated in current mode. Transient response of 60 kV operated X-ray showed an increase in current on the incidence of X-rays on the detector and detector response is found linear in the studied dose range from 74 µGy/s to 307 µGy/s.

Zhao et al. (Zhao et al., 2016) demonstrated that the resistivity of a sample could be increased by annealing at higher temperatures which will drastically affect X-ray response. ZnO crystals annealed at 300-900 ^{0}C showed an increase in their resistivity due to increased V_O, V_{Zn} and O_i defects as confirmed by Photoluminescence. X-ray sensors are fabricated by depositing 100 nm Al electrodes on both sides of the crystal. The dark current and current at different dose rates for X-rays were measured, which showed a non-linear response at lower dose rates and a linear response at higher dose rates. The response of the single crystal was compared with ZnO thin films, showing a similar behavior at lower dose rates. This non-linearity is attributed to the presence of traps, affecting the carrier lifetime of highly resistive ZnO. The detector was also evaluated using a 10 ps electron beam pulse produced from Tsinghua Thomson Scattering X-ray source and the transient response is measured by recording photocurrent. Photocurrent rise time was ~ 0.8 ns and fall time ~ 3.3 ns which showed that ZnO detector can be used to detect ultrafast pulsed nuclear radiation.

2.8.2 ZnO based Transparent Ceramics

Transparent ceramics are alternative to single crystals and fabricated by powder materials by subjecting it under high pressure 80-90 MPa and temperature ~1000 ^{0}C for several hours. It leads to the diffusion of particles and significant grain growth. Another method of preparing transparent ceramic is by spark plasma sintering (SPS) in which powder is heated by passing a high current ~5000A in pulses and subjected to pressure as applied in a uniaxial hot press.

ZnO undoped and doped with various impurities such as Zn, Ga, Ga & N, In and Li ceramics scintillator are reported and their extensive characterizations such as SEM, PL, X-ray luminescence are carried out to evaluate material's properties. V. A. Demidenko et al. 2007 (Demidenko et al., 2007) reported Zn doped ZnO ceramic preparation using uniaxial hot pressing. The developed ceramic has good transparency. It emits 380 & 500 nm emission when excited with X-rays. This 380 nm emission corresponds to near band edge emission, whereas 500 nm corresponds to the green emission associated with Zn vacancy. The X-ray exposed ceramic sample also shows thermally stimulated luminescence (TSL) at temperature corresponding to 0.21eV, a trap energy state in ZnO. E.I. Gorokhowa et al. 2008 (Gorokhova et al., 2008) reported four types of ZnO based ceramic scintillators: two of which are based on undoped ZnO, prepared from extra pure ZnO and the other two are doped, i.e., ZnO:Ga and ZnO:Ga,N ceramics prepared using uniaxial hot pressing. The undoped ceramic ZnO_{II} has high light yield (LY) ~9050 photon/MeV. The doping of Ga and Ga&N resulted in a drastic decrease in LY to 4020 photon/MeV, but the luminescence falloff time reduced to 1 ns from 10 ns in undoped ZnO because NBE emission only in Ga doped ZnO while undoped ZnO has additional 510 nm defect band emission characteristics. The ratio of NBE to DBE emission can changed by modifying the doping concentration of Ga and N. Similar developments on ZnO

and ZnO:Ga with 0–0.1% Ga concentration ceramic samples are also reported, showing DBE emission for ZnO~580 nm and NBE emission for ZnO:Ga~389 nm (Gorokhova et al., 2018).

Neal et al. reported the preparation of ZnO and ZnO:Ga ceramic by hot pressing and SPS method (Neal et al., 2009). The developed ceramics are showing mixed NBE and DBE emissions. The luminescence property has improved after the H_2 treatment of these ceramic samples. P.A. Rodnyi et al. reported the fabrication of ZnO (Rodnyi et al., 2012b; a), ZnO:Li, ZnO:Zn, ZnO:Ga (Rodnyi et al., 2012a) and ZnO:In (Rodnyi and Venevtsev, 2019) using uniaxial hot press. The synthesized ZnO ceramic samples with 300-600 nm particle sizes are subjected to 100-200 MPa pressure and 900-1100 ^{0}C temperature under vacuum to achieve 1-1.5 mm thick samples with large 5-30 μm size grains, in resultant transparent ceramics for 400 nm and higher wavelengths.

Alpha excited radioluminescence of developed ceramic scintillator characteristics is comparable to Yettrium Aluminum Perovskite (YAP) scintillator using a ^{241}Am source. ZnO and ZnO:Li, ZnO:Ga and ZnO:Zn ray excited luminescence, alpha and gamma pulse height spectra were studied using ^{241}Am and ^{137}Cs radiation sources. The responses are compared with that of CsI as a standard detector. The light yield of ZnO ceramic as compared to CsI was 57%. Scintillation decay times were reduced by doping of Li or Ga compared to undoped ZnO, making it a fast scintillator as required in imaging applications (Rodnyi et al., 2012a). ZnO:Zn transparent ceramic produced by the hot pressing method emits 380 nm and 500 nm photons after X-ray excitations (Rodnyi et al., 2012a). ZnO:In ceramic X-ray, luminance showed fast decay time ~1 ns, similar to ZnO:Ga ceramic detectors.

Grigorjeva et al. reported the fabrication of ZnO, and ZnO:Al (Grigorjeva et al., 2010) using high-temperature sintering (HT) and high-pressure low-temperature sintering of the corresponding nanoparticle grown by plasma method and two other ZnO ceramics using high-temperature sintering of ZnO nanoparticle grown by pulsed electron beam evaporation and solar physical vapor deposition(SPVD) (Grigorjeva et al., 2017). In HT, a pellet of nanoparticles is prepared by applying pressure ~290 MPa and annealed in air at ~1200 ^{0}C. In HPLT, sintering is done in high pressure ~8 GPa and low temperature ~150 ^{0}C. ZnO:Al ceramic is synthesized using HT, which results in a large grain size of 100 nm-5μm with a very fast excitonic decay (<1ns). Luminescence kinetics of HT and HPLT grown ZnO ceramic show the faster decay time of HPLT ceramics; however, the light yield is low compared to HT ceramic.

2.8.3 ZnO Thin/Thick Film Detectors

Zinc Oxide thin films prepared using liquid phase epitaxy (LPE), Magnetron sputtering and screen printing methods are investigated for an alpha, gamma, X-rays and proton detection. T. Yanagida et al., 2010 reported the development of ZnO:In thin film by LPE. The c-axis oriented ZnO:In films of 10mmx10 mmx0.5mm dimension are grown on ZnO single crystal substrates using LPE furnace (Sekiwa et al., 2010). The concentrations of Indium in ZnO varied from 26-141 ppm. Alpha excited responses are studied using ^{241}Am alpha radiation source. Alpha radio-luminescence spectra show peaks at 375 nm near band edge emissions and 520 nm near defect-related emissions. As the concentrations of In increase, the intensity of alpha radio-luminescence spectra decreases, and a similar observation is noticed for the alpha pulse height spectrum.

ZnO:Ga thin film developed using magnetron sputtering is reported for their pulsed radiation detection application (Ma et al., 2010). The response of the developed film has been studied with pulse X-ray, proton, gamma and single alpha radiations. ZnO:Ga films of 50 mm diameter and 50-micron thickness are prepared on alumina substrate using ZnO and Ga_2O_3 (0.01 mol%) followed by annealing at 800 ^{0}C. The rapid annealing of RF magnetron sputtered

ZnO:Ga films shows the enhanced light yield compared to as-grown ZnO:Ga films. The two-step sputtered grown thick film showed light yield much higher than similar thick films fabricated in one step and light yield for two-step grown thick films is comparable to that of a single crystal of ZnO:Ga (Choi et al., 2008)

Fujimoto et al. prepared ZnO:Cu scintillator films using the LPE method (Fujimotoy et al., 2014). ZnO and 0.3 mol% CuO powder were melted in an LPE furnace and deposited on a ZnO substrate by cooling and rotating the substrate. Photoluminescence and alpha radio-luminescence spectra showed the enhanced emission in the green region due to donor-acceptor recombination (figure 20b). The luminescence decay time was estimated to be 2.3 μs, which is comparatively larger than ZnO:Ga, because of defect-related luminescence. The developed film's light yield is very high compared to BGO, which makes it excellent scintillator material for alpha radiation detection.

Arshak et al. 2005 reported the fabrication of ZnO thick film on P<100> Si wafers using the screen printing method, which acts as a radiation-sensitive p-n junction (Arshak et al., 2005). 92 wt% of ZnO was mixed in 8 wt% PVB and thus, a polymer paste was prepared for screen printing on Si wafers followed by a heat treatment at 393 K for two hours. The addition of doping of 0.1 wt% of carbon improved the gamma dose-response by generating more charge carriers. Silver contacts are printed on the device to make a radiation-sensitive diode of area 100 mm x 100mm x 50 μm thickness. The device is then exposed to 662 keV gamma radiations at different doses and radiation damage is estimated using I-V characteristics. I-V plots for ZnO/Si diode at different gamma exposure (0-511 μSv) show a drastic change in current under reverse bias at dose 171 μSv. The normalized current at applied voltages ±4 V showed that the current is increasing at different doses. Thus, ZnO/Si diodes may be suitable for dosimetry applications in the investigated range.

Another capacitive device is prepared using the above-mentioned ZnO+PVB polymers paste using screen printing on interdigitated Ag electrode over alumina substrate. The device is exposed to ^{137}Cs (662 keV) gamma-radiation. In real-time, change in capacitance was monitored using capacitive interface module circuitry (Arshak et al., 2006) consisting of temperature sensor, 24- bit SD regulator, digital filter and serial interface integrated on a single chip. The measured changes in capacitance of ZnO at different gamma doses, 0-30 mGy, showed a significant change in the capacitance at 1-2.5 mGy. No significant change was observed at lower dose 0-1 mGy and higher doses, i.e., > 2.5 mGy. Thus, such devices can be used in the 1-2.5 mGy range. Also, the device is reusable as the device exposure history can be removed by annealing the sensor at 150 ^0C for few hours in the oven.

2.8.4 Zinc Oxide Powder Scintillator

The scintillating nature of ZnO as powder phosphor was reported long back by W Lehman (Lehmann, 1965, 1966, 1971). ZnO:Ga doped powder is synthesized by the firing of ZnO and Ga_2O_3 powder in the open air, followed by annealing in a hydrogen environment, which makes it luminescent by taking oxygen, leaving excess Zn in ZnO. Photoluminescence at different temperatures showed increased emissions peak, shifted towards lower energy. The fluorescence decay time of the phosphor was in ~ns range.

Zinc oxide powder scintillator is usually fabricated by a solid-state reaction between Ga_2O_3 and ZnO, followed by annealing in the H_2 environment. The diffusion of Ga metal in ZnO has been reported for its application in associated particle imaging, which requires detector having decay time of the order of ns (Bourret-Courchesne et al., 2009). ZnO:Ga powder is prepared in three-step: (i) mixing of stoichiometric ratio of Ga_2O_3 and ZnO, (ii) annealing of the mixture at 900 – 1100^0C under high vacuum for 15 hrs and (iii) final annealing is carried out in reducing

environment of H_2+Ar gas at 800 ^{0}C. It results in a luminous ZnO:Ga scintillator showing photoluminescence emission at 389 nm. Here, emission in the green region is suppressed significantly due to Ga doping. Fast luminescence decay ~0.8 ns is observed when excited with X-rays. In the second synthesis method, a mixture of Ga metal (0.04 mol%) and ZnO is subjected to 1200 ^{0}C for 12 hrs. Photoluminescence characterization showed an NBE emission and a broad emission in the green region attributed to the oxygen vacancies created due to excess diffusion of Ga at Zn sites. The X-ray excited luminescence decay is much slower than ZnO:Ga powder prepared with the earlier method, whereas the X-ray excited luminosity is also reduced to 27 % for solid-state reaction synthesized ZnO:Ga.

Commercial ZnO:Ga powder by four different manufacturers, i.e., NETech, GK31, WL1201 and LBNL3518 were used to make a scintillation screen with the help of a binder. Photoluminescence, X-ray excited luminescence and alpha radiation pulse height analysis characterizations showed that LBNL3518 phosphor acts as a fast scintillator when excited by alpha radiation with the weakest visible emission and the height of the light output(Neal et al., 2006). ZnO:Ga powder mixed with potassium silicate binder and an electrolyte was coated on optical face plates using gravity settling method and is used to detect 3.5 MeV alpha particle in a portable neutron generator that uses D-T reaction for the production of neutron (Hausladen et al., 2005). Alpha particles emitted opposite to neutrons in D-T reactions were detected with 90% efficiency.

Further, scintillation screens are prepared using ZnO:Zn powder mixed with ^{6}LiF in ratio 2:1 to make ZnO:Zn/^{6}LiF scintillator for the detection of thermal neutron radiation (Sykora et al., 2018). The photoluminescence spectrum shows the emission centered around 505 nm. X-ray and alpha radioluminescence show peaks at 400 nm and 505 nm, respectively. X-ray radioluminescence is relatively broadened towards a higher wavelength than alpha radiation due to difference in interaction range. Pulse height spectra show that the maximum amplitude of ZnO:Zn/^{6}LiF is half of that compared with ZnS:Ag/^{6}LiF. Pulse shape analysis showed a clear distinction between gamma and neutron pulses. It can be used to measure count rate six times higher than ZnS:Ag/^{6}LiF due to low afterglow compared with ZnS:Ag/^{6}LiF and thus, a good candidate to replace the conventional ZnS:Ag/^{6}LiF detector.

ZnO:Ga powder prepared using solution-phase method, urea precipitation and combustion method used to prepare transparent ceramic (Neal et al., 2009). Solution phase synthesis was performed by drop-wise addition of KOH in zinc acetate dihydrate and gallium oxide solution in methanol at 60^{0}C. In urea precipitation, ZnO:Ga powder is obtained by the exothermic precipitation using urea in a solution of ZnO and Ga_2O_3 in water and nitric acid followed by thermal treatment at 900^{0}C. In Combustion synthesis, a solution of ZnO and Ga $(NO_3)_{2\ in}$ glycine is heated till combustion, followed by heat treatment at 500^{0}C. The synthesized powders were characterized using XRD, TEM and photoluminescence measurements. These results suggest that the finest grain size can be achieved in the solution phase compared to the other two processes and PL measurement showed the mixed NBE and DBE emissions. The ratio of NBE to DBE has improved after H_2 treatment of powder samples.

2.8.5 ZnO Nano-composite Detector

Nanocomposite scintillator consists of nanoparticle dispersed in a transparent polymer matrix. Nanoparticles can be acquired commercially or prepared using different synthesis techniques. The matrix should be transparent in order to transmit the light generated due to the interaction of radiation with the scintillator to PMT. Various organic materials such as polystyrene, PMMA, polysulphone, Epoxy are used as a matrix for preparing nano-composites. Energy from ionizing radiation is transferred to the matrix, non-radiatively transferred to scintillator employing Forster energy resonance transfer (FRET) and finally, scintillation

photons are emitted due to radiative transitions. ZnO nanocomposite is reported for several applications such as UV detection, ultrasonics and other application (Alamdari et al., 2019b; Jassim et al., 2016). ZnO:Ga nanocomposite scintillators are reported for the detection of X-rays and alpha particles. Hana Burešová et al. 2016(Burešová et al., 2016) prepared ZnO:Ga/PS nanocomposite by dispersing ZnO:Ga nanoparticles 10% by weight to polystyrene followed by compacting in a steel dye. X-ray radioluminescence shows the emission of 391 nm due to Ga doping in ZnO. The absence of 300-350 nm polystyrene emission indicates the non-radiative transfer of energy from the polymer matrix to ZnO:Ga particles. The scintillation performance was studied using X-rays. X rays first transfer energy to the polymer matrix, which is non-radiatively transferred to ZnO:Ga particles, showing 391 nm luminescence.

S. Alamdari et al. 2019 reported the preparation of ZnO and ZnO:Ga nanoparticles using the sol-gel method (Alamdari et al., 2019a). ZnO and ZnO's prepared powder was mixed in polystyrene and ethanol solution keeping PS and powder ratio ~0.7 and stirred for mixing. The solution is then poured on a glass plate and dried at room temperature for 24 hours. Photoluminescence of such nanocomposite sample shows intense blue emission, attributed to the Ga doping. The highest counting efficiency ~49.95% was obtained for GZO-3 (11 mg/cm^2) nanocomposite.

2.8.6 ZnO Nanorod/Nanowire based Detectors

ZnO nanorods are a one-dimensional structure and are explored for active and passive type detectors for ionizing radiation. Vertically aligned nanorods grown by a hydrothermal process are suggested as good materials for scintillator applications due to their optical and fast response characteristics (Angub et al., 2018). ZnO:Ga nanorods scintillator using low-temperature hydrothermal method were prepared for photoluminescence and alpha-induced pulse height spectra(Kurudirek et al., 2018, 2016).

Kobayashi et al. 2015 prepared vertically aligned nanowires by electrodeposition on GZO substrate and explored them for X-ray imaging applications (Kobayashi et al., 2015). The developed scintillator has PL emission ~3.2 eV, which can be seen in contrast with ZnO/GZO scintillator emitting visible radiation at 2 eV. The performance of the scintillator is evaluated using 20 kV X-ray imaging from the synchrotron radiation facility. A good spatial resolution is observed in comparison with an undoped ZnO layer scintillator. Qianli Li et al. 2018 (Li et al., 2018a) reported ZnO and ZnO's preparation on quartz substrate by hydrothermal method. They used RF magnetron sputtering for synthesizing seed layer, followed by a dip in the solution of $Zn(NO_3)_2 \cdot 6H_2O$, $Ga(NO_3)_3 \cdot xH_2O$ and HMTA kept at 95 ^{0}C (Li et al., 2016, 2018b). Further, H_2 treatment reduced ZnO's visible emission and, thus, improved NBE emission, making it a fast scintillator. X-ray imaging was carried out using 20 kV X-rays and about 1µm spatial resolution was demonstrated.

Another application of ZnO nanorods is gamma-ray detection by measuring the material's damage through structural, optical or any other physical properties after exposure to high doses of gamma radiation. The impact of gamma radiation on structural and optical properties of ZnO nanowire is studied by A. Reyhani et al.,2018 (Reyhani et al., 2018). ZnO nanowires are prepared using the oxidation of Zn metal film prepared using thermal evaporation of Zn metal in the air on a glass substrate. ZnO thin films of different thicknesses i.e. 125 nm, 250 nm and 500 nm were exposed to 100 kGy of gamma dose and radiation effects were studied by scanning electron microscopy showing the gamma radiation-induced damage to ZnO nanorwires. X-ray diffraction studies revealed the increase in average diameter of nanowire together with the onset of (100) peak in XRD pattern of ZnO nanowire after gamma radiation exposure. It suggests the formation of Zn metal due to gamma exposure. UV-Vis spectroscopy showed reduced transmittance and bandgap due to gamma exposure. These changes are attributed to

the formation of Zn metal and oxygen vacancies due to exposure and the improved yellow-green emission.

2.8.7 ZnO Nano-phosphor TL/OSL detectors

Zinc Oxide scintillator gives an instant light signal after interacting with ionizing radiation. Thus, ZnO-based material can act as storage phosphors, different from scintillator in the sense that phosphor trap electron-hole pair produced after the interaction of the ionizing radiation and need stimulation to recombine at some luminescent centre. The stimuli may be either thermal or optical, making nano-phosphor as TL/OSL dosimeter. Various methods are used to prepare zinc oxide nano materials for phosphor applications such as sol-gel, chemical synthesis, combustion method, etc.

A.J. Reddy et al. (Jagannatha Reddy et al., 2011; Reddy et al., 2012) prepared ZnO nano phosphor by low-temperature combustion method followed by calcination at high temperature (Jagannatha Reddy et al., 2011). A solution of zinc nitrate with oxalyldihydrazide as fuel is prepared in water and subjected to a temperature of 300 ^{0}C. The green luminescence signature decreases with increasing the calcination temperature, which assists in the removal of Zn_i and V_o defects because of oxygen absorption. TL readout shows a peak at 343 ^{0}C after exposure to gamma radiation in the range 10-50 Gy. This TL peak is attributed to the recombination of charge carriers released from oxygen interstitial defects. A single TL peak in the glow curve has the advantage of low fading and simpler to analyze for dosimetry applications. This material can be used for high-temperature radiation dosimetry. Fe doped ZnO prepared using combustion method is studied for high dose gamma dosimetry. TL measurements of 1-5 kGy gamma irradiated ZnO:Fe nanoparticles showed a single peak glow curve at ~368 ^{0}C, which increases with dose.

ZnO nanophosphor synthesized using a similar method with 500 nm-2 micron particles is reported for its application in beta radiation dosimetry (V. R. Orante-Barrón et.al., 2015)(Orante-Barrón et al., 2015). ZnO nanophosphor prepared by making solution of zinc nitrate and glycine as fuel and subjected to 200 ^{0}C to remove water and at 500 ^{0}C for combustion to make ZnO nanoparticles. The prepared powder is annealed in air at 900 ^{0}C and exposed to ^{90}Sr beta radiation at different doses in 12.5 Gy-400 Gy range. TL measurements are investigated and the respective glow curve showed two peaks at 149 ^{0}C and 308 ^{0}C. The two different peaks correspond to shallow and deep trap electron recombination centers, respectively. The high-temperature TL peak can be used for dosimetry applications. The response in the studied range of dose is linear. The fading of 25% in 9h after exposure is noticed because of low-temperature peak and such materials can be used for radiotherapy and food irradiation applications.

U. Pal et al. (Pal et al., 2006, 2008) prepared ZnO and ZnO:Yb nano phosphor by glycol mediated chemical reaction. Ethylene glycol and zinc acetate solution heated at 440 K for 2h. Yb is doped by adding $YbCl_3.6H_2O$ in the solution. TL analysis of 100 Gy beta radiation-exposed sample shows that undoped ZnO has two TL peaks at 420 K and 490 K. The Yb doping in ZnO modifies the glow curve to a single peak ~490 K, but the sensitivity is reduced about six times. Such luminescence quenching is observed in X-ray-induced TL in Fe doped ZnO nanoparticles (Srivastava et al., 2009). ZnO and ZnO:Yb show linear TL response in dose range 0-100 Gy for beta radiation. The doping of Yb also reduces the afterglow and TL fading (Pal et al., 2008).

C. Cruz-Vázquez et al. (Cruz-Vázquez et al., 2007, 2010, 2014) prepared undoped ZnO and ZnO:Mg nanophosphor using thermal oxidation of ZnS and chemical synthesis route to study TL/OSL properties. ZnO pellet obtained by thermal annealing of chemical bath deposition (CBD) prepared zinc sulphide at 700^{0}C in air for 24 hrs. Thermal oxidation of ZnS results in the

development of zinc oxide ZnO pellets exposed to beta dose from 0.5 to 10.5 kGy and linear TL signature is observed in the studied range, making it suitable for high dose beta radiation dosimetry. Also, a preliminary OSL decay curve at 600 Gy exposed sample is reported and OSL counts are linear at different doses(Cruz-Vázquez et al., 2007). ZnO nanophosphor pellet is synthesized by chemical reaction of zinc chloride, thiourea and sodium hydroxide followed by drying in a vacuum and compressing at 0.5 tons using a hydraulic press. Beta TL studied in 25-6400 Gy range showed a TL peak ~230 ^{0}C and response is linear in the studied range. About 22% fading is observed in 96 hrs (Cruz-Vázquez et al., 2010). The doping of Mg in the above chemical reaction is achieved by adding the right stoichiometric ratio of magnesium chloride in the source precursor solution. Thus, a ZnO:Mg pellet is obtained(Cruz-Vázquez et al., 2014). Thermoluminescence shows a prominent TL peak at 480 K (207^{0}C) after exposing to 25-2500 Gy, showing its usefulness for dosimetry applications and two less intense peaks are observed at 397 K (124^{0}C) and 635 K (362^{0}C). The peak shifts towards lower temperature with increasing dose from 25 to 2500 Gy. The counts obtained at dose 100 Gy exposure shows repeatable nature and a linear variation to dose up to 1600 Gy followed by the saturation in response with any further increase in dose. The fading of ZnO:Mg TL data is 25% in 2 days.

Soares et al. reported the preparation of ZnO nanocrystal using the co-precipitation method followed by calcination at 900-1000 ^{0}C for 2 hrs. TL and OSL characteristics are studied for the beta radiation in 0.08-40.6 Gy dose range. TL response depends on the sintering temperature. The 900^{0}C sintered ZnO shows a broad TL peak~ 370^{0}C, whereas 1000^{0}C sintered ZnO two peaks at 144^{0}C and 308^{0}C. The minimum detectable dose (MDD) for a TL is 492µG. TL/OSL intensity increases with dose. LM-OSL shows a broad peak consisting of three peaks when deconvoluted (figure 39 c) and CW –OSL shows exponential decay curve at different doses. MDD obtained from CW-OSL ~100 mGy, which is less as compared to TL. The change in TL glow curve due to sintering temperature is linked with the PL emission at that temperature, suggesting that 900^{0}C sintering suppresses the green emission whereas 1000^{0}C sintering promotes green emission.

Borbón-Nuñez et al.2014(Borbón-Nuñez et al., 2014) prepared zinc oxide pellets using chemical bath deposition(Cruz-Vázquez et al., 2010). The pellets are further sintered at different temperatures such as 1123 K, 1173 K and 1223 K. These pellets were exposed to different beta doses using ^{90}Sr source and various detection characteristics such as glow curve linearity, reproducibility and fading are investigated. The glow curve shows that pellets sintered at 1173 K and 1223 K have better sensitivity than that of 1123 K. Further, the glow curve shows multiple peaks at three different temperatures ranging from 412 K to 600 K. The most sensitive peak observed at higher temperature facilitates its use for high temperature applications. TL counts are linear in studied 25-800 Gy dose range and are highly reproducible. Fading study shows the loss of 25%, 28% and 45% TL signal in 96 h for these three sintered samples. Considering the sensitivity and fading and the 1173 K sintered ZnO sample shows optimum TL response. Burruel-Ibarra et al. 2013 (Burruel-Ibarra et al., 2013) prepared ZnO phosphor by thermal annealing of ZnS obtained from the chemical method for beta detection in 0.025-6.4 kGy range. Thermoluminescence measurements show two prominent peaks at 94 ^{0}Cand 341 ^{0}C. The response is linear with the dose; however, fading is 48% in 6 hrs. The fading is very high as compared to ZnO prepared by Borbón-Nuñez et al.2014.

Recently Avilés-Monrea et al. 2018 reported ZnO:Na using Cruz-Vazquez et al. (Cruz-Vázquez et al., 2014) chemical method except the doping of Na in place of Mg. The TL properties are studied for beta radiation in 0.08-2048 Gy range. The glow curve for undoped ZnO is modified significantly by Na doping. TL peaks obtained by 50Gy beta exposure are at 140^{0}C and 320^{0}C. In the dose range 0.08-1 Gy, the second peak is observed at 347^{0}C with higher intensity. The integrated TL is linear with the dose in this range. The first peak intensity at

140^0C is higher than the second peak in 1-2048 Gy dose range. The response is linear up to 256 Gy and saturates afterward. The fading of TL is ~ 26% in four days, which is relatively lower than the earlier reported phosphors. The sensitivity for ZnO:Na is 200 times higher than other ZnO phosphors, prepared by the same method. Table 2.6 summarizes the ZnO-based materials with respective synthesis processes and characteristics investigated for TL/OSL dosimeter applications.

Table 2.6: Summary of ZnO based Detector for Ionizing Radiation Measurement

Structure	Material	Growth Method	Raw Materials	Characterization	Properties	Application	Ref
Single crystal	ZnO ZnO:Ga ZnO:Li ZnO:In,Li and ZnO:Er,Li	Pressure melt (Modified Bridgeman Method)	ZnO melt with do pants	PL, Alpha RL	NBE and defect luminescence emission Fast decay time ~ ns-µs	Scintillator	(Nause and Nemeth, 2005) (Neal et al., 2008)
	ZnO	Hydro-thermal	ZnO dissolved in LiOH+ KOH	PL and XRD Alpha Imaging	Sharp peak~ 3.37 eV, Highly pure Image of Alpha source obtained	Scintillator	(Maeda et al., 2005) (Yanagida et al., 2010)
	ZnO:Sc	Hydro-thermal	ZnO+0.3 % Sc2O3	PL, XRD Alpha RL Pulsed radiation detection	Sharp peak~ 377 nm, Broad peak~ 556 nm Alpha pulse height spectrum time response ~162-170 ns and fall time ~300-326 ns	Scintillator	(Zuo et al., 2011) (Zhang et al., 2014)
	ZnO	Hydro-thermal	--	Photo current measurement X ray dosimeter	Linear in dose rate range 74-307 µGy/s	Ionization	(Endo et al., 2011)
	ZnO		Annealed ZnO crystal at 900^0C	Photo current measurement Ultra-fast pulsed X ray detector	rise time ~0.8 ns fall time~3.3 ns	Ionization	(Zhao et al., 2016)
Transparen	ZnO:Zn	UHP	ZnO:Zn	X- ray	Emission peaks at	Scintillat	(Demidenk

t ceramic			powder	Luminescence and TSL	380 nm and 500 nm Trap depth 0.21 eV by TSL corresponding Zn impurity	or	o et al., 2007)
	ZnO I ZnO II ZnO:Ga ZnO:Ga, N	UHP	ZnO (VHP and SP), Ga_2O_3 and Ga $(NO_3)_3$	PL, XRL	Highest light yield in ZnOII~9050 photon/MeV, lowest in ZnO:Ga and ZnO: Ga, N ~420 photon/MeV XRL emission 520 nm for ZnO I and ZnO II, 395nm and 510 nm for ZnO:Ga and ZnO:Ga, N Fall off time ~10 ns for ZnO and 1ns for ZnO:Ga and 3.3ns for ZnO:Ga, N	Scintillator	(Gorokhova et al., 2008),
	ZnO ZnO:Ga	Uniaxial Hot Press SPS	Undoped ZnO and ZnO:Ga powder	Photo-luminescence Before and after H2 treatment	Mixed emission of NBE and Visible. H2 treatment enhanced luminescence maintain NBE to visible ratio	scintillator	(Neal et al., 2009)
	ZnO and ZnO:Al	HT HPLT	ZnO and ZnO:Al NPs by Plasma Method	SEM, PL	Large grain size ~100 nm-5µm ZnO:Al fast excitonic decay (<1ns) ZnO (HPLT) luminescence kinetics faster than ZnO (HT) but low light yield	Scintillator	(Grigorjeva et al., 2010)
	ZnO, ZnO:Zn, ZnO:Li and ZnO:Ga	UHP	ZnO, ZnO:Zn, ZnO:Li and ZnO:Ga Powder Particle size ~90-700 nm	Photoluminescence X-ray luminescence (XRL) Alpha and gamma Pulse height spectra	XRL Emission of 2.37 eV photon corresponding Vzn in undoped ZnO. Light yield (for gamma) ~ 57% of CsI (Tl) and decay time 1.6µs. ZnO:Zn. XRL emission 2.10-2.53 eV ZnO:Li XRL shows little difference with undoped ZnO, Fast decay (17ns, 60-70%) and light yield 25%	Scintillator	(Rodnyi et al., 2012a)

					of CsI(Tl) for alpha radiation. ZnO:Ga XRL shows 3.21 eV NBE only. fast decay~1ns Light yield decreases 2% as compared to undoped ZnO		
	ZnO	HT	ZnO nano powder by PEBE and SPVD	X rays RL, TSL	Emission consists of peaks at 2.10–2.16 eV and2.33–2.35 eV. TSL main Peaks 410 K and 380 K TSL linear in 3-9 kGy	Scintillator	(Grigorjeva et al., 2017)
	ZnO and ZnO:Ga	UHP	ZnO ZnO+Ga_2O_3 0-0.1 mol%	PL, XRL	ZnO PL emission ~580 nm, ZnO:Ga emission~389 nm ZnO:Ga luminescence damping ~1.1ns-10 ns	Scintillator	(Gorokhova et al., 2018)
	ZnO:In	UHP	ZnO powder With In	XRL	X ray luminescence emission 388 nm NBE only and decay time ~1ns.	Scintillator	(Rodnyi and Venevtsev, 2019)
	ZnO:In Thin Film	LPE	ZnO+ In_2O_3 Concertation 26, 53 and 141 ppm	Alpha pulse height analysis Alpha Radio-luminescence	Higher sensitivity at In doping (26ppm) Emission peaks 375 nm and 520 nm	Scintillator	J.S. Neal et.al. (Sekiwa et al., 2010)
Thin Film	ZnO:Ga	Magnetron Sputtering	ZnO and Ga_2O_3 (0.01 mol%)	Alpha time response Pulsed Proton detection and energy response X ray time and energy response	Alpha Rise time ~320 ns, FWHM~686 ps Pulse obtained due (p,γ) reaction, Luminescence increases sharply up to 8 MeV and slower thereafter Flat energy response above 40 keV	Scintillator	(Ma et al., 2010)

	ZnO:Cu	LPE	ZnO+CuO (0.3 mol%)	Photoluminescence Alpha radio luminescence and pulse height analysis	Increased PL and RL emission in green region Light yield very high 140% compared to that of BGO	Scintillator	(Fujimotoy et al., 2014)
	ZnO:Ga	RF Magnetron Sputtering	ZnO + 1 mol% Ga_2O_3 on sapphire annealing of sample to high temperature (800-900)	Alpha radio-luminescence	Radio luminescence improved by rapid thermal annealing light yield of two step sputtered film is higher compared to single crystal	Scintillator	(Choi et al., 2008)
Thick Film	ZnO/Si pn-junction	Screen Print	ZnO+PVB (8%) on Si substrate	I-V Measurement Change in Normalized Current	Change observed in dose range 0-511 µSv	Damage detector	(Arshak and Korostynska, 2002)
	ZnO with Inter-digitated Electrode	Screen Print	ZnO+PVB/Al_2O_3	Capacitance Measurement	Change observed in 1-2.5 mGy	Damage	(Arshak et al., 2006)
Powder	ZnO:Ga	Solid State Reaction	ZnO +Ga_2O_3 And H2 annealing	PL at different temperature	Emission peak shift at different temperature Faster Response compared undoped ZnO	Luminescent Screen	(Lehmann, 1966)
	ZnO:Ga	(i) Solid State Reaction (ii) Diffusion of Ga Metal	ZnO+ Ga_2O_3 ZnO +Ga Metal	PL and Luminescence decay time	Emission 389 nm, decay time~0.8ns Green Emission due to oxygen vacancy and slower as compared with ZnO:Ga obtained from solid state process	Ultra-fast alpha scintillator	(Bourret-Courchesne et al., 2007)

		in ZnO					
	ZnO:Ga	Commercial powder by NETech, GK31, WL1201 and LBNL 3518	ZnO and Ga_2O_3	PL, X ray Luminescence Alpha Pulse height spectrum	LBNL3518 phosphor has weakest emission in visible range, fastest luminescence decay time LBNL phosphor ~1.1 ns (97%) and highest light output when excited by alpha	Alpha particle detector	(Neal et al., 2006)
	ZnO:Ga	Commercial powder NETech	film on fused fibre optic plate using Gravity settling with potassium silicate binder	Pulse height analysis	Pulse height spectrum can be distinguished with background. Efficiency was estimated ~90%	Alpha detection in D-T reaction	(Hausladen et al., 2005)
	ZnO:Zn /^{6}LiF	ZnO:Zn Commercial powder +^{6}LiF	Scintillator screen 2:1 ZnO:Zn and 6LiF	PL, XL and Alpha RL Pulse height and pulse analysis with neutron /gamma	PL centred at 505 nm Radioluminescence emission ~390 nm, 505 nm Pulse height shows light out is 50% of that of ZnS/6LiF Pulse shape analysis shows clear discrimination of neutron and gamma	Thermal Neutron Detector	(Sykora et al., 2018)
	ZnO:Ga	Solution phase, Urea Precipitation and Combustion synthesis Followed by H2 Treatment	SP- ZAD + Ga_2O_3 in methanol UP- ZnO+ Ga_2O_3 solution urea CS - ZnO+ $Ga(NO_3)_2$ in glycine	XRD, TEM Photo-luminescence	Fine particle obtained in Combustion synthesis Mix emission of fast NBE and slow visible emission. NBE to visible ratio improved after H2 treatment	Scintillator	(Neal et al., 2009)

Nano-composite	ZnO:Ga /PS	Photo induced precipitation Mixed with PS and compressed	ZnO:Ga Nano powder PS granules	PL ad XRL	PL Emission~391 nm Fast XRL ~0.5 ns	Scintillator, X ray detection	(Burešová et al., 2016)
	ZnO:Ga /PS	sol-gel method Mixed with PS+ ethanol solution	ZnO:Ga nano powder PS, Ethanol	XRL and Alpha pulse height spectra	Blue XRL emission Highest efficiency~49.5% with thickness~11 mg/cm2	Scintillator, Alpha detector	(Alamdari et al., 2019a)
Nano rods	ZnO and ZnO:Ga /Glass	Low temperature hydrothermal method	$(Zn(NO_3)_2$, $Ga(NO_3)_3$ HMTA, NH4OH Sodium citrate	XRD, PL, Alpha and Gamma pulse height spectra	Vertical Nanorods, 380 nm emission, Sensitive to Alpha radiation	Alpha detector	(Kurudirek et al., 2018, 2016)
Nano rod array	ZnO and ZnO:Ga	Hydrothermal	$(Zn(NO_3)_2 \cdot 6H_2O$ $Ga(NO_3)_3 \cdot xH2O$ HMTA	XRD, PL, X ray Imaging	Vertical nanorods, Visible emission suppressed by hydrogen annealing making Fast 1 µm spatial resolution obtained	X ray imaging	(Li et al., 2016, 2018a; b)
Nano wire	ZnO/GZO	Electro deposition	Aquas solution of Zinc nitrate hydrate	PL, X ray imaging using synchrotron facility	Emission ~3.2 eV Good spatial resolution	X ray imaging	(Kobayashi et al., 2015)
Nanowire	ZnO/Glass	Thermal Evaporation	Zn Metal in air	XRD, SEM, UV-Vis spectroscopy (100 kGy Gamma Exposure)	Zn metal formation 100 Peak, Decrease in Band gap, improvement in yellow green region	Gamma Damage detector	(Reyhani et al., 2018)

	ZnO	Solution Combustion	$Zn(NO_3)_2 \cdot 6H_2O$ and $C_2H_6N_4O_2$	PL, Gamma TL measurement 10-50 Gy	PL emission ~420 nm TL Single peak ~ 343 ^{0}C	Gamma Dosimetry	(Jagannatha Reddy et al., 2011)
	ZnO:Fe	Solution Combustion	$Zn(NO_3)_2 \cdot 6H_2O$ $C_2H_6N_4O_2$ and $Fe(NO_3)_3$	Gamma TL Dose range- 1-5 kGy	TL Single peak ~ 368^{0}C Linear TL response	Gamma dosimetry	(Reddy et al., 2012)
	ZnO	Solution Combustion Method	$Zn(NO_3)_2 \cdot 6H_2O$ and $C_2H_5NO_2$	TL analysis by exposing sample ^{90}Sr beta source Dose range- 12.5 Gy-400 Gy	TL peak ~149 ^{0}C and 308 ^{0}C , Linear TL response Fading ~25% in 2 days	Beta dosimetry	(Orante-Barrón et al., 2015)
	ZnO ZnO:Yb	Glycol mediated chemical synthesis	$(C_2H_3O-)_2Zn$ ethylene glycol $YbCl_3 \cdot 6H_2O$	Beta TL analysis 100 Gy dose	ZnO TL Peaks~420 K and 490 K ZnO:Yb TL peak ~490 K Linear in 1-100 Gy	Beta dosimetry	(Pal et al., 2006)
	ZnO	Thermal Oxidation of ZnS	ZnS	Beta TL & OSL Dose range- 0.5-10.5 kGy (TL) 40-600 Gy (OSL).	TL peak~ (200^{0}C, broad, for sample sintered at 700^{0}C) Linear TL/OSL response	Beta dosimetry	(Cruz-Vázquez et al., 2007)
	ZnO	Chemical method	$ZnCl_2$,$CS(NH_2)_2$NaOH	Beta TL in dose range 25-6400 Gy	TL peak~ 230^{0}C (broad, depends upon dose), Linear Response, Fading 22% in 96 hours	Beta dosimetry	(Cruz-Vázquez et al., 2010)

	ZnO:Mg	Chemical Reaction	$ZnCl_2$,CS(NH_2)2NaOH and $MgCl_2$	Beta TL in dose range 25-2500 Gy	TL Peak~ 207^0C (changes with dose) Linear up 1600Gy then sublinear Fading ~25% in 2 days	Beta dosimetry	(Cruz-Vázquez et al., 2014)
	ZnO Nanocrystals	Co-Precipitation	$Zn(NO_3)_2.6H_2O$ And KOH	Beta TL of 900^0C and 1000^0C sintered ZnO Dose range- 0.08-40.6 Gy CW and LM OSL PL at different sintering temperature	TL Peaks~ 370 ^{0}C (Tsint~900^0C), TL peaks ~144 ^{0}C and 308^0C (Tsint~1000^0C) Minimum detectable dose (MDD)~492µGy (TL) LM-OSL consist of 3 peaks when de-convoluted CW-OSL intensity increases with dose, MDD (OSL)~100 mGy	Beta dosimetry	(Soares et al., 2017)
	Sintered ZnO	Chemical Method /Sintering	$ZnCl_2$,CS(NH_2)$_2$NaOH	Beta TL of ZnO sintered at 1123 K, 1173 K and 1223 K Dose range - 25-800 Gy	Three TL Peaks ~412K-600K depending upon dose Linear response, Fading 25-48% in 96 h ZnO sintered at 1173 K response is optimum compared to other		(Borbón-Nuñez et al., 2014)

2.9 Titanium Oxide for Sensor Applications

Titanium Dioxide (TiO_2) is a transition metal oxide that crystallizes in three forms Rutile, Anatase and Brookite as shown in Fig 2.24. Rutile is the most stable form of TiO_2 and has a tetragonal structure. Anatase and Brookite phase are in tetragonal and orthorhombic and are metastable, obtained by heating rutile phase 600-800 ^{0}C (Greenwood and Eranshaw, 1984). In the Rutile phase, Titanium is surrounded by six oxygen in an octahedral arrangement and oxygen is surrounded by three Titanium atoms in trigonal planer coordination (figure 2.24a) (Khataee and Mansoori, 2012a). Because of the low surface energy requirement, the growth along [001] direction is preferred and can be seen in nanorods. Rutile TiO_2 is commonly used in photocatalytic and dilute magnetic semiconductors due to its large bandgap of 3.06 eV. It is one of the highest refractive index materials (n=2.613). Its anatase phase is used as semiconductor due to the large bandgap of 3.2 eV. Since rutile and anatase have large bandgaps, so they have the property to block UV radiation also. Bulk TiO_2 is used to provide whiteness in products such as paints, coatings, plastics, paper, inks, medicines, toothpaste etc. Bulk TiO_2 is found in two forms i.e., single-crystalline and polycrystalline (powder) forms.

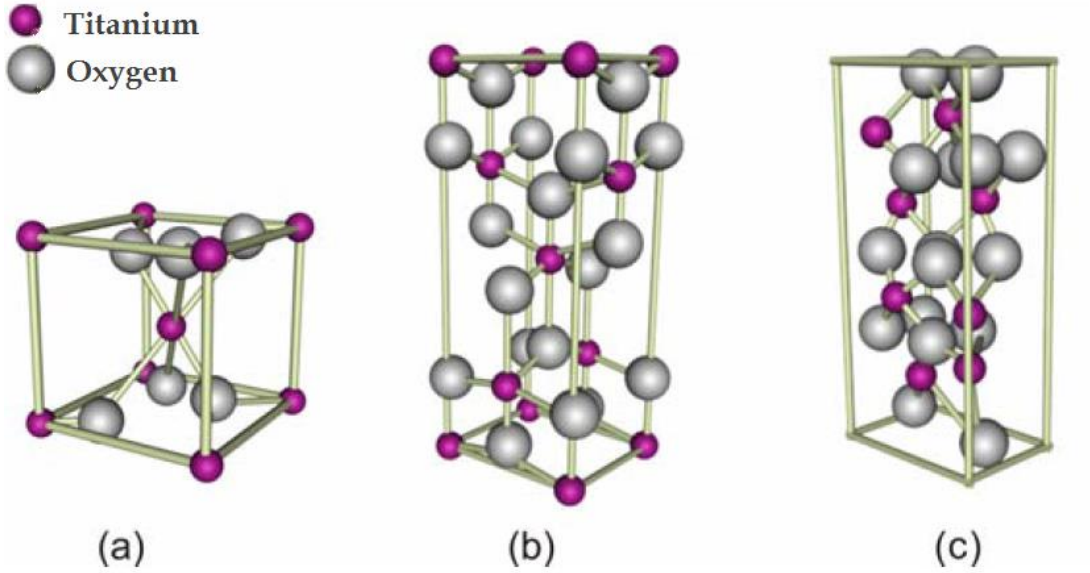

Figure 2.24:Unit Cell of (a) Rutile (b) anatase and (c) Brookite (Khataee and Mansoori, 2012a)

Titanium dioxide (TiO_2) is low cost, nontoxic material and widely used as a metal oxide semiconductor for various applications such as hydrogen production by high photo-catalytic ability (Chiarello et al., 2017), photovoltaic cells (Bai et al., 2014), sensing applications (Bai and Zhou, 2014), treatment of cancer (Selin and Cigir, 2019), antimicrobial (Jadiyappa, 2012) and UV protection (Trivedi and Murase, 2017). TiO_2 nanostructures can be synthesized using various methods such as Sol-gel, CVD, electrochemical, hydrothermal (Khataee and Mansoori, 2012b), thus providing flexibility in manipulating their geometrical shape and sizes for different applications.

TiO_2 in ionizing radiation sensing applications is also reported in some reports. Gamma radiation measurements can be performed by studying the gamma-induced alteration in physical and optical properties. TiO_2:Mn nanoparticle preparation and thermoluminescence of gamma exposed sample reported. TiO_2 nanoparticle prepared using co-precipitation method using $TiOSO_4$ and $MnCl_2.6H_2O$ precursors. Thermoluminescence glow curves recorded by exposing to gamma radiation of 10 Gy (^{137}Cs) showed the prominent peak at 240 ^{0}C along with

two peaks at 220 ^{0}C and 258 ^{0}C, which usually disappeared within 2 hr. The sensitivity of TiO_2:Mn to TLD-100 commercial dosimeter is 0.5 and the response is linear with the dose up to 100Gy. It showed fading ~20% within 2 hrs together with repeatability within ±3% (Azorín-Vega et al., 2007). TiO_2 nanoparticles were prepared by co-precipitation method using $TiCl_4$ and NaOH precursor in different ratios 1:2, 1:3 and 1:4 and calcined at different temperature 450-550^{0}C. Gamma radiation exposure was given to these samples 200Gy-1kGy. Main glow curves obtained around 245 ^{0}C and 255 ^{0}C and TL response increases with gamma dose (Sharmila et al., 2019). Concentrated TiO_2 sols are reported for gamma radiation dosimetry. The change in UV absorption of TiO_2 sols by exposure to gamma radiation is a measure of gamma radiation dose. TiO_2 sols prepared by hydrolysis of TTIP and condensation at room temperature. Sol sample exposed to 0.2 -1.6 kGy of gamma radiation showed absorption of 540 nm wavelength, which is correlated with exposed gamma radiation dose (Huang et al., 2001). Gamma radiation effects on optical and luminescence properties are also studied (Gui-Ang et al., 2014). TiO_2 thin films prepared on glass substrate by RF magnetron sputtering. These developed films were exposed to gamma radiation 2-80 kGy. UV-vis spectroscopy of the exposed samples shows enhanced absorption near 400 nm and showed a new absorption edge at 430 nm on 80 kGy exposure. The optical band gap decreases from 3.3 to 2.9 eV as the exposure increases from 2 to 80 kGy. Photoluminescence emission intensity of the TiO_2 film was also found to decrease with gamma radiation dose (Gui-Ang et al., 2014). Gamma radiation effects on optical and electrical properties are investigated (Janu et al., 2008; Roy et al., 2008). TiO_2 doped Lead Phthalocyanine (PbPc) and Chloro-aluminium phthalocyanine (ClAlPc) on ITO substrate Optical and electrical characteristics studied by exposing to gamma radiation 10-800 mR and 1-10 Gy, respectively. Optical bandgap and forward current decreased because of defect formation in devices due to gamma radiation exposure. Table 2.7 summarize the TiO_2 structures for radiation sensing applications.

Table 2.7: Summary of TiO_2 as Ionizing radiation sensor

Material	**Growth Method**	**Properties**	**Application**	**Ref**
TiO_2:Mn Nanoparticles	Co-precipitation	Gamma Themo-luminesce glow peak ~2400^{0}C, linear response 10-80 Gy, ±3%	TL dosimeter	Azorín-Vega et al., 2007
TiO_2 Nanoparticles	Co-Precipitation	Gamma TL glow curve~ 245^{0}C and 255^{0}C, Dose range 200Gy-1kGy	TL Dosimeter	Sharmila et al., 2019)
TiO_2 Sols	Sol-gel	Increased UV absorption with dose Dose range 0.2-1.6 kGy	Damage Detector	Huang et al., 2001)
TiO_2 Thin Film	Sputtering	Increased UV absorption Decreasing of Band gap and PL Dose range: 2-80kGy	Damage Detector	Gui-Ang et al., 2014
TiO_2 doped PbPc	Blend and Spin coating	Band Gap and Forward current decreases with dose Dose range: 10-800 mR	Dosimeter	Janu et al., 2008
TiO_2 doped ClAlPc	Blend and Spin coating	Band Gap and Forward current decreases with dose Dose range: 1-10Gy	Dosimeter	Roy et al., 2008

2.10 Summary

To summarize, ionizing radiations are high-energy electromagnetic waves or particles capable of ionizing matter. Electromagnetic radiation (X-ray, Gamma-ray) typically interacts via photoelectric absorption, Compton scattering and pair production depending on the energy of the radiation. Charged particles such as alpha, beta radiation interaction results in ionization and excitation of the medium's atom. Neutrons interact by capture, elastic scattering and inelastic scattering. All interaction leads to the production of charges which further ionizes the media and ultimately deposits the radiation energy in the medium. In the case of biological organisms like humans, exposure to radiations results in damage to the cell, leading to several health hazards depending on the dose deposited in the body. It makes the requirement of a detector for sensing the radiation. Several materials and mechanisms have been evolved for the detection of such radiation. Ionization, Scintillation, Stimulated luminescence and damages are four important mechanisms for detecting and measuring radiation. Zinc oxide is one such material that has unique properties which can be utilized for all four mechanisms. For ionization detectors, bulk single crystal has been demonstrated for X-ray measurement. For scintillation applications bulk single crystal, single-crystalline film, transparent ceramic and composites can be utilized. ZnO nano phosphor is used for TL/OSL measurement for beta /gamma dosimetry and some studies of structural and optical properties of gamma-irradiated ZnO nanowire have been reported. TiO_2 is another wide bandgap material explored for radiation measurement using the thermoluminescence method, change in optical and electrical properties.